

# Synthetic Analogues of the Active Site of the A-Cluster of Acetyl Coenzyme A Synthase/CO Dehydrogenase: Syntheses, Structures, and Reactions with CO

Todd C. Harrop,<sup>†</sup> Marilyn M. Olmstead,<sup>‡</sup> and Pradip K. Mascharak<sup>\*,†</sup>

Department of Chemistry and Biochemistry, University of California, Santa Cruz, California 95064, and Department of Chemistry, University of California, Davis, California 95616

Received November 28, 2005

Two metallocenones, namely  $(\text{Et}_4\text{N})_2[\text{Ni}(\text{NpPepS})]$  (**1**) and  $(\text{Et}_4\text{N})_2[\text{Ni}(\text{PhPepS})]$  (**2**) containing carboxamido-N and thiolato-S as donors have been used to model the bimetallic  $\text{M}_p\text{--Ni}_d$  subsite of the A-cluster of the enzyme acetyl coenzyme A synthase/CO dehydrogenase. A series of sulfur-bridged Ni/Cu dinuclear and trinuclear complexes (**3–10**) have been synthesized to explore their redox properties and affinity of the metal centers toward CO. The structures of  $(\text{Et}_4\text{N})_2[\text{Ni}(\text{PhPepS})]$  (**2**),  $(\text{Et}_4\text{N})[\text{Cu}(\text{neo})\text{Ni}(\text{NpPepS})]\cdot 0.5\text{Et}_2\text{O}\cdot 0.5\text{H}_2\text{O}$  (**3**),  $(\text{Et}_4\text{N})[\text{Cu}(\text{neo})\text{Ni}(\text{PhPepS})]\cdot \text{H}_2\text{O}$  (**4**),  $(\text{Et}_4\text{N})_2[\text{Ni}\{\text{Ni}(\text{NpPepS})\}_2]\cdot \text{DMF}$  (**5**),  $(\text{Et}_4\text{N})_2[\text{Ni}(\text{DMF})_2\{\text{Ni}(\text{NpPepS})\}_2]\cdot 3\text{DMF}$  (**6**),  $(\text{Et}_4\text{N})_2[\text{Ni}(\text{DMF})_2\{\text{Ni}(\text{PhPepS})\}_2]$  (**8**), and  $[\text{Ni}(\text{dppe})\text{Ni}(\text{PhPepS})]\cdot \text{CH}_2\text{Cl}_2$  (**10**) have been determined by crystallography. The  $\text{Ni}_d$  mimics **1** and **2** resist reduction and exhibit no affinity toward CO. In contrast, the sulfur-bridged Ni center (designated  $\text{Ni}_c$ ) in the trinuclear models **5–8** are amenable to reduction and binds CO in the Ni(I) state. Also, the sulfur-bridged  $\text{Ni}_c$  center can be removed from the trimers (**5–8**) by treatment with 1,10-phenanthroline much like the “labile Ni” from the enzyme. The dinuclear Ni–Ni models **9** and **10** resemble the  $\text{Ni}_p\text{--Ni}_d$  subsite of the A-cluster more closely, and only the modeled  $\text{Ni}_p$  site of the dimers can be reduced. The Ni(I)–Ni(II) species display EPR spectra typical of a Ni(I) center in distorted trigonal bipyramidal and distorted tetrahedral geometries for **9**<sub>red</sub> and **10**<sub>red</sub>, respectively. Both species bind CO, and the CO-adducts **9**<sub>red</sub>-CO and **10**<sub>red</sub>-CO display strong  $\nu_{\text{CO}}$  at 2044 and 1997  $\text{cm}^{-1}$ , respectively. The reduction of **10** is reversible. The CO-affinity of **10** in the reduced state and the  $\nu_{\text{CO}}$  value of **10**<sub>red</sub>-CO closely resemble the CO-bound reduced A-cluster ( $\nu_{\text{CO}} = 1996 \text{ cm}^{-1}$ ).

## Introduction

Acetyl coenzyme A synthase/carbon monoxide dehydrogenase (ACS/CODH) is a bifunctional metalloenzyme that catalyzes two important biological reactions, namely the reversible reduction of  $\text{CO}_2$  into CO (CODH activity) and the synthesis of acetyl coenzyme A (acetyl CoA) from CO,  $\text{CH}_3$  from a methylated corrinoid iron–sulfur protein, and the thiol CoA (ACS activity).<sup>1,2</sup> Once formed, acetyl

CoA is converted into cell carbon or respired as acetate depending on the metabolic needs of the cell. This enzyme is present in a number of anaerobic bacteria including acetogens, methanogens, and sulfate-reducers that utilize the Wood–Ljungdahl pathway for autotrophic carbon fixation.<sup>3</sup> Indeed, ACS/CODH has been implicated in the chemotrophic origin of life in which primitive organisms consumed CO or  $\text{CO}_2$  from volcanic or hydrothermal sites for the formation of carbon–carbon bonds.<sup>4</sup> Interest in ACS/CODH stems from its unusual metallocuster active sites, its role in the global carbon cycle (reducing the levels of gaseous pollutants such as  $\text{CO}_2$ ), and the reactions it catalyzes

\* To whom correspondence should be addressed. E-mail: pradip@chemistry.ucsc.edu. Fax: + 1-831-459-2935. Tel: + 1-831-459-4251.

<sup>†</sup> University of California, Santa Cruz.

<sup>‡</sup> University of California, Davis.

(1) (a) Ragsdale, S. W. *Crit. Rev. Biochem. Mol. Biol.* **2004**, *39*, 165–195. (b) Ragsdale, S. W.; Kumar, M. *Chem. Rev.* **1996**, *96*, 2515–2539.

(2) Lindahl, P. A. *Biochemistry* **2002**, *41*, 2097–2105.

(3) Wood, H. G.; Ljungdahl, L. G. *Variation in Autotrophic Life*; Academic Press: New York, 1991.

(4) Huber, C.; Wächtershäuser, G. *Science* **1997**, *276*, 245–247.

utilizing well-known organometallic ligands such as CO and CH<sub>3</sub>, analogous to the industrial Monsanto acetic acid process.

Although a large volume of spectroscopic and biochemical data was available for the enzyme for some time,<sup>1,2</sup> the site of acetyl CoA synthesis (A-cluster) has come under intense scrutiny following the publication of three high-resolution crystal structures.<sup>5–7</sup> The A-cluster of ACS/CODH has been shown to exist in two different oxidation states, A<sub>ox</sub> (*S* = 0) and A<sub>red</sub>-CO (*S* = 1/2), the one electron reduced CO-adduct formed under CO atmosphere. The paramagnetic A<sub>red</sub>-CO state is readily identified by a strong rhombic EPR signal (*g* = 2.08, 2.07, and 2.03) that exhibits dipolar broadening when isotopically substituted with <sup>61</sup>Ni, <sup>57</sup>Fe, or <sup>13</sup>CO (hence referred to as the NiFeC signal).<sup>1,8</sup> In addition, A<sub>red</sub>-CO displays a strong band in its IR spectrum at 1996 cm<sup>-1</sup> (*ν*<sub>co</sub>) consistent with a terminally bound CO molecule.<sup>9</sup> Addition of CH<sub>3</sub><sup>+</sup> to CO-treated ACS/CODH affords a diamagnetic state, although the order of CO and CH<sub>3</sub><sup>+</sup> binding is still debatable.<sup>10</sup> Titration of ACS/CODH with the bidentate chelator 1,10-phenanthroline (phen) results in the removal of ~30% of the Ni present in the enzyme.<sup>11</sup> Such removal of “labile Ni” abolishes the NiFeC signal and also shuts down acetyl CoA synthesis with no effect on CODH activity. Reconstitution of phen-treated enzyme with NiCl<sub>2</sub> replenishes both the NiFeC signal and synthase activity.<sup>11</sup> These results strongly suggest that “labile Ni” is a requirement for ACS activity.

Crystallographic studies on ACS/CODH from the acetogenic bacterium *Moorella thermoacetica* (formerly known as *Clostridium thermoaceticum*) have revealed some interesting and unexpected features never seen before in any metalloenzyme. The overall α<sub>2</sub>β<sub>2</sub> protein comprises several metalloclusters in the different subunits.<sup>5,6</sup> The β subunits at the center of the protein contain the B, C, and D clusters, the site of CODH activity (C-cluster). The α-subunits, located at the terminal ends of the protein, contain the A-cluster, the site responsible for acetyl CoA formation. Interestingly, the structure of the A-cluster reported by two separate groups turned out to be quite different even though the enzyme was isolated from the same organism (*M. thermoacetica*). The

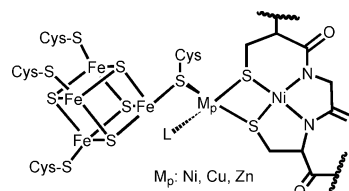


**Figure 1.** Schematic of the A-cluster site of ACS/CODH from *Moorella thermoacetica*. M<sub>p</sub>: Ni(II), Cu(I), or Zn(II); L is a nonprotein ligand.

first structure of ACS/CODH reported by Drennan and co-workers revealed a homodimeric α<sub>2</sub>β<sub>2</sub> protein whose active site is relatively unexposed to solvents and contains a trio of different metals present at the A-cluster.<sup>5</sup> The A-cluster in the Drennan structure consists of an Fe<sub>4</sub>S<sub>4</sub> cubane bridged through one Cys-S residue to a bimetallic site that contains a square-planar Ni(II) (Ni<sub>d</sub>, distal to Fe<sub>4</sub>S<sub>4</sub>) ion with N<sub>2</sub>S<sub>2</sub> coordination derived from two backbone carboxamido nitrogens and two Cys-S residues. The Ni<sub>d</sub> site is further bridged through two Cys-S donors to a tetrahedral Cu(I) (M<sub>p</sub>, proximal to Fe<sub>4</sub>S<sub>4</sub>) center. A fourth nonprotein ligand is also bound to Cu(I) to complete the coordination sphere (Figure 1). The second structure by Fontecilla-Camps and co-workers, however, revealed a very different A-cluster site.<sup>6</sup> First, the α<sub>2</sub>β<sub>2</sub> quaternary structure is no longer symmetric and consists of an α<sub>c</sub>ββ<sub>o</sub> structure in which one of the α-subunits (α<sub>o</sub>) is more open and exposed to solvent. In the A<sub>o</sub>-cluster of α<sub>o</sub>, a square-planar Ni(II) ion occupies the M<sub>p</sub> site that is ~20 Å removed from a closed CO tunnel. Quite in contrast, the other α subunit (α<sub>c</sub>) is closed off to solvent and a tetrahedral Zn(II) ion resides at the M<sub>p</sub> site (Figure 1). This A<sub>c</sub>-cluster is located at the end of an open hydrophobic CO tunnel from the C-cluster. The discrepancy in the structures of the A-cluster from the same enzyme triggered an intense debate regarding the identity of the true catalytic metal ion at the M<sub>p</sub> site. The debate has recently subsided after careful biochemical<sup>11a,12,13</sup> and computational studies.<sup>14,15</sup> It is now evident that Ni at the M<sub>p</sub> site is required for the ACS activity. A very recent structural study on an ACS/CODH from the hydrogenogenic bacterium *Carboxydothermus hydrogenoformans* has also revealed the presence of Ni at the M<sub>p</sub> site.<sup>7</sup>

The extent to which the unusual coordination architecture of the A-cluster dictates its ability to assemble acetyl CoA is still an unanswered question. The presence of carboxamido-N donors at the Ni<sub>d</sub> site is quite uncommon in biology. At this time, coordination of deprotonated carboxamido-N has only been observed in the oxidized P-cluster of nitrogenase,<sup>16</sup> nitrile hydratase<sup>17</sup> (which contains a similar Cys–

- (5) Doukov, T. I.; Iverson, T. M.; Seravalli, J.; Ragsdale, S. W.; Drennan, C. L. *Science* **2002**, *298*, 567–572.
- (6) Darnault, C.; Volbeda, A.; Kim, E. J.; Legrand, P.; Vernède, X.; Lindahl, P. A.; Fontecilla-Camps, J. C. *Nat. Struct. Biol.* **2003**, *10*, 271–279.
- (7) Svetlitchnyi, V.; Dobbek, H.; Meyer-Klaucke, W.; Meins, T.; Thiele, B.; Römer, P.; Huber, R.; Meyer, O. *Proc. Natl. Acad. Sci. U.S.A.* **2004**, *101*, 446–451.
- (8) (a) George, S. J.; Seravalli, J.; Ragsdale, S. W. *J. Am. Chem. Soc.* **2005**, *127*, 13500–13501. (b) Seravalli, J.; Kumar, M.; Ragsdale, S. W. *Biochemistry* **2002**, *41*, 1807–1819. (c) Xia, J.; Hu, Z.; Popescu, C. V.; Lindahl, P. A.; Münck, E. *J. Am. Chem. Soc.* **1997**, *119*, 8301–8312. (d) Ragsdale, S. W.; Wood, H. G.; Antholine, W. E. *Proc. Natl. Acad. Sci. U.S.A.* **1985**, *82*, 6811.
- (9) Chen, J.; Huang, S.; Seravalli, J.; Gutzman, H., Jr.; Swartz, D. J.; Ragsdale, S. W.; Bagley, K. A. *Biochemistry* **2003**, *42*, 14822–14830.
- (10) (a) Tan, X. S.; Sewell, C.; Lindahl, P. A. *J. Am. Chem. Soc.* **2002**, *124*, 6277–6284. (b) Barondeau, D. P.; Lindahl, P. A. *J. Am. Chem. Soc.* **1997**, *119*, 3959–3970.
- (11) (a) Bramlett, M. R.; Tan, X.; Lindahl, P. A. *J. Am. Chem. Soc.* **2003**, *125*, 9316–9317. (b) Shin, W.; Lindahl, P. A. *J. Am. Chem. Soc.* **1992**, *114*, 9718–9719.

- (12) Seravalli, J.; Xiao, Y.; Gu, W.; Cramer, S. P.; Antholine, W. E.; Krymov, V.; Gerfen, G. J.; Ragsdale, S. W. *Biochemistry* **2004**, *43*, 3944–3955.
- (13) (a) Funk, T.; Gu, W.; Friedrich, S.; Wang, H.; Gencic, S.; Grahame, D. A.; Cramer, S. P. *J. Am. Chem. Soc.* **2004**, *126*, 88–95. (b) Gencic, S.; Grahame, D. A. *J. Biol. Chem.* **2003**, *278*, 6101–6110.
- (14) Webster, C. E.; Darensbourg, M. Y.; Lindahl, P. A.; Hall, M. B. *J. Am. Chem. Soc.* **2004**, *126*, 3410–3411.
- (15) (a) Brunold, T. C. *J. Biol. Inorg. Chem.* **2004**, *9*, 533–541. (b) Schenker, R. P.; Brunold, T. C. *J. Am. Chem. Soc.* **2003**, *125*, 13962–13963.
- (16) Peters, J. W.; Stowell, M. H. B.; Soltis, M.; Finnegan, M. G.; Johnson, M. K.; Rees, D. C. *Biochemistry* **1997**, *36*, 1181–1187.

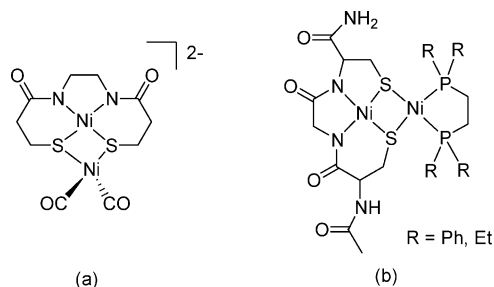
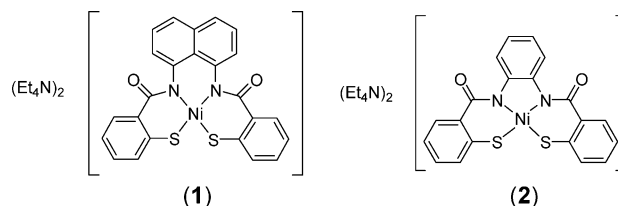


**Figure 2.** Structures of (a)  $[\{\text{Ni}(\text{CO})_2\}\{\text{NiS}_2\text{N}'_2\}]^{2-}$  and (b)  $[\text{Ni}(\text{CGC})\text{-Ni}(\text{dRpe})]$ .

X-Cys metal-binding motif as the  $\text{Ni}_d$  site), and most recently in Ni-SOD.<sup>18</sup> Since the publication of the first structure of ACS/CODH, several low-molecular-weight models of the ACS site have been synthesized and studied to determine the intrinsic properties of the metal-containing active site(s).<sup>19–25</sup> In these pursuits, researchers have focused mostly on the bimetallic  $\text{M}_p\text{-Ni}_d$  site of ACS and ignored the  $\text{Fe}_4\text{S}_4$  portion (unlikely site of substrate binding). For example, Rauchfuss and co-workers have synthesized the model complex  $[\{\text{Ni}(\text{CO})_2\}\{\text{NiS}_2\text{N}'_2\}]^{2-}$  (structure a, Figure 2) with two terminal CO ligands bound to the bridged Ni center in the 0 oxidation state.<sup>24</sup> This complex was the first example of a structurally characterized, mixed-valence, sulfur-bridged, dinuclear Ni model containing carboxamido-N coordination that resembles the CO-bound form of the enzyme. More recently, Riordan and co-workers have employed the metallopeptide unit  $[\text{Ni}(\text{CGC})]^{2-}$  to synthesize biologically relevant Ni-Ni models such as  $[\text{Ni}(\text{CGC})\text{Ni}(\text{dRpe})]$  (structure b, Figure 2).<sup>20a</sup> Although phosphine donors are not present in the enzyme, they do allow for more favorable reduction of the  $\text{Ni}_p$  site of the model to the Ni(I) state and binding of CO (as shown by electrochemistry). However, none of the models from this study has been characterized further by structural and spectroscopic (such as EPR, FTIR) studies. Clearly, more model complexes are required to establish the properties of the active site(s) of the ACS A-cluster and what implications these have on the overall mechanism of acetyl CoA synthesis.

As part of our continuing efforts on modeling the bimetallic  $\text{M}_p\text{-Ni}_d$  portion of the A-cluster of ACS, we describe herein the syntheses and properties of several di/trinuclear metal complexes utilizing the dicarboxamido-dithiolato Ni(II) metallosynthons  $(\text{Et}_4\text{N})_2[\text{Ni}(\text{NpPepS})]$  (**1**)<sup>26</sup> and  $(\text{Et}_4\text{N})_2\text{-}$



$[\text{Ni}(\text{PhPepS})]$  (**2**) reported by us in preliminary accounts.<sup>27</sup> The redox behavior of two Cu(I)–Ni(II) models, namely  $(\text{Et}_4\text{N})[\text{Cu}(\text{neo})\text{Ni}(\text{NpPepS})]$  (**3**) and  $(\text{Et}_4\text{N})[\text{Cu}(\text{neo})\text{Ni}(\text{PhPepS})]$  (**4**) clearly demonstrate that the catalytically active A-cluster cannot utilize Cu(I) at the  $\text{M}_p$  site. The four trinuclear models  $(\text{Et}_4\text{N})_2[\text{Ni}\{\text{Ni}(\text{NpPepS})\}_2]$  (**5**),<sup>27b</sup>  $(\text{Et}_4\text{N})_2\text{-}[\text{Ni}(\text{DMF})_2\{\text{Ni}(\text{NpPepS})\}_2]$  (**6**),<sup>27b</sup>  $(\text{Et}_4\text{N})_2[\text{Ni}\{\text{Ni}(\text{PhPepS})\}_2]$  (**7**), and  $(\text{Et}_4\text{N})_2[\text{Ni}(\text{DMF})_2\{\text{Ni}(\text{PhPepS})\}_2]$  (**8**) and the two dinuclear models  $[\text{Ni}(\text{terpy})\text{Ni}(\text{NpPepS})]$  (**9**)<sup>27a</sup> and  $[\text{Ni}(\text{dppe})\text{Ni}(\text{PhPepS})]$  (**10**)<sup>27a</sup> provide the opportunity to study, for the first time, a series of complexes with variable donor sets and coordination geometries at the bridged Ni(II) center ( $\text{Ni}_p$  mimics). In this paper, we report the results of redox studies and CO binding at the  $\text{M}_p$  ( $\text{M} = \text{Cu}, \text{Ni}$ ) centers of these models and compare the spectral data of the reduced CO-adducts with that of the  $\text{A}_{\text{red}}\text{-CO}$  ( $S = 1/2$ ) signal of the enzyme in order to establish the mode of CO binding by the A-cluster of ACS/CODH.

## Experimental Section

Thiosalicylic acid, 1,2-phenylenediamine, 1,8-diaminonaphthalene, triethylamine,  $[\text{Ni}(\text{dppe})\text{Cl}_2]$ , CuCl,  $[\text{Cu}(\text{MeCN})_4]\text{PF}_6$ , 2,9-dimethyl-1,10-phenanthroline (neocuproine, abbreviated as neo), 2,2':6',2''-terpyridine (terpy), 1,2-ethanedithiol (edt), and 1,10-phenanthroline (phen) were purchased from Aldrich Chemical Co. and used without further purification. NpPepSH<sub>4</sub> (*N,N'*-naphthalenebis(*o*-mercaptobenzamide),<sup>26</sup> 2,2'-dithiosalicyl chloride,<sup>26</sup>  $(\text{Et}_4\text{N})_2\text{-}[\text{Ni}(\text{NpPepS})]$ <sup>26</sup> (**1**),  $(\text{Et}_4\text{N})_2[\text{NiCl}_4]$ ,<sup>28</sup>  $[\text{Cu}(\text{neo})\text{Cl}]$ ,<sup>29a</sup>  $(\text{Na})_3[\text{Cu}_3(\text{edt})_3]$ ,<sup>29b</sup> and  $[\text{Ni}(\text{terpy})\text{Cl}_2]$ <sup>30</sup> were synthesized by following published procedures. All manipulations were carried out under  $\text{N}_2$  (where needed) using Schlenk lines or drybox techniques. The solvents were purified by standard techniques and distilled prior to use.

**Synthesis of Compounds. PhPepSH<sub>4</sub> (*N,N'*-Phenylenebis(*o*-mercaptobenzamide)).** The synthesis of the ligand comprises the following steps.

- (17) (a) Harrop, T. C.; Mascharak, P. K. *Acc. Chem. Res.* **2004**, *37*, 253–260. (b) Mascharak, P. K. *Coord. Chem. Rev.* **2002**, *225*, 201–214. (c) Nagashima, S.; Nakasako, M.; Dohmae, N.; Tsujimura, M.; Takio, K.; Odaka, M.; Yohda, M.; Kamiya, N.; Endo, I. *Nat. Struct. Biol.* **1998**, *5*, 347–351. (d) Huang, W.; Jia, J.; Cummings, J.; Nelson, M.; Schneider, G.; Lindqvist, Y. *Structure* **1997**, *5*, 691–699.
- (18) (a) Barondeau, D. P.; Kassmann, C. J.; Bruns, C. K.; Tainer, J. A.; Getzoff, E. D. *Biochemistry* **2004**, *43*, 8038–8047. (b) Wuerger, J.; Lee, J.-W.; Yim, Y.-I.; Yim, H.-S.; Kang, S.-O.; Carugo, K. D. *Proc. Natl. Acad. Sci. U.S.A.* **2004**, *101*, 8569–8574.
- (19) Rao, P. V.; Bhaduri, S.; Jiang, J.; Holm, R. H. *Inorg. Chem.* **2004**, *43*, 5833–5849.
- (20) (a) Krishnan, R.; Riordan, C. G. *J. Am. Chem. Soc.* **2004**, *126*, 4484–4485. (b) Krishnan, R.; Voo, J. K.; Riordan, C. G.; Zahkarov, L.; Rheingold, A. L. *J. Am. Chem. Soc.* **2003**, *125*, 4422–4423.
- (21) Hatlevik, Ø.; Blanksma, M. C.; Mathrubootham, V.; Arif, A. M.; Hegg, E. L. *J. Biol. Inorg. Chem.* **2004**, *9*, 238–246.
- (22) Wang, Q.; Blake, A. J.; Davies, E. S.; McInnes, E. J. L.; Wilson, C.; Schröder, M. *Chem. Commun.* **2003**, 3012–3013.
- (23) Golden, M. L.; Rampersad, M. V.; Reibenspies, J. H.; Darensbourg, M. Y. *Chem. Commun.* **2003**, 1824–1825.
- (24) Linck, R. C.; Spahn, C. W.; Rauchfuss, T. B.; Wilson, S. R. *J. Am. Chem. Soc.* **2003**, *125*, 8700–8701.
- (25) Harrop, T. C.; Mascharak, P. K. *Coord. Chem. Rev.* **2005**, *249*, 3007–3024.

- (26) Harrop, T. C.; Olmstead, M. M.; Mascharak, P. K. *Inorg. Chim. Acta* **2002**, *338*, 189–195.
- (27) (a) Harrop, T. C.; Olmstead, M. M.; Mascharak, P. K. *J. Am. Chem. Soc.* **2004**, *126*, 14714–14715. (b) Harrop, T. C.; Olmstead, M. M.; Mascharak, P. K. *Chem. Commun.* **2004**, 1744–1745.
- (28) Gill, N. S.; Taylor, F. B. *Inorg. Synth.* **1967**, *9*, 136–143.
- (29) (a) Healy, P. C.; Pakawatchai, C.; White, A. H. *J. Chem. Soc., Dalton Trans.* **1985**, 2531–2539. (b) Rao, C. P.; Dorfman, J. R.; Holm, R. H. *Inorg. Chem.* **1986**, *25*, 428–439. (c) Anderson, O. P.; Brito, K. K.; Laird, S. K. *Acta Cryst.* **1990**, *C46*, 1600–1603.
- (30) Judge, J. S.; Reiff, W. M.; Intille, G. M.; Ballway, P.; Baker Jr., W. A. *J. Inorg. Nucl. Chem.* **1967**, *29*, 1711–1716.



**Step 1. (PhPepS)<sub>2</sub>.** A solution of 1,2-phenylenediamine (0.23 g, 2.13 mmol) and triethylamine (0.67 g, 6.63 mmol) dissolved in 10 mL of CH<sub>2</sub>Cl<sub>2</sub> was quickly added to a solution of 2,2'-dithiosalicyl chloride (0.72 g, 2.10 mmol) in 10 mL of CH<sub>2</sub>Cl<sub>2</sub>. The resulting pale yellow-brown solution was stirred for 48 h at room temperature. This solution was then washed with aqueous NaHCO<sub>3</sub> and NaCl. The CH<sub>2</sub>Cl<sub>2</sub> layer was dried with MgSO<sub>4</sub> and filtered, and the solvent was removed by rotary evaporation to yield an oily yellow residue. The oil was triturated three times with Et<sub>2</sub>O (10 mL) to afford a pale yellow solid. Yield: 0.32 g (41%). <sup>1</sup>H NMR (298 K, CDCl<sub>3</sub>, 500 MHz): (ppm from TMS) 8.59 (s, 1H, NH), 7.67 (d, 1H), 7.53 (t, 1H), 7.39 (m, 2H), 7.21 (m, 2H). Selected IR bands (KBr matrix, cm<sup>-1</sup>): 3217 (m, ν<sub>NH</sub>), 1652 (vs, ν<sub>co</sub>).

**Step 2. PhPepSH<sub>4</sub>.** To a degassed THF solution (10 mL) of (PhPepS)<sub>2</sub> (0.32 g, 0.85 mmol) was slowly added solid NaBH<sub>4</sub> (0.17 g, 4.49 mmol) in small portions at 4 °C. The bright yellow-orange solution was then allowed to stir at room temperature for 16 h. Next, the THF solution was concentrated to ~10% of the original volume via short-path vacuum distillation and 6 M acetic acid was added dropwise at 4 °C until the pH was 3. The light cream-colored solid that precipitated almost immediately upon addition of acid was collected by filtration, washed with degassed water, and dried on a high-vacuum line for 2 h. Yield: 0.30 g (90%). <sup>1</sup>H NMR (298 K, CDCl<sub>3</sub>, 500 MHz): (ppm from TMS) 8.73 (s, 1H, NH), 7.69 (d, 1H), 7.56 (t, 1H), 7.36 (d, 1H), 7.31 (t, 1H), 7.22 (m, 2H), 4.53 (br s, 1H, SH). Selected IR bands (KBr plates, cm<sup>-1</sup>): 3300 (m, ν<sub>NH</sub>), 2552 (w, ν<sub>SH</sub>), 1652 (vs, ν<sub>co</sub>).

**(Et<sub>4</sub>N)<sub>2</sub>[Ni(PhPepS)] (2).** A batch of NaH (0.054 g, 2.24 mmol) was added to a solution of PhPepSH<sub>4</sub> (0.17 g, 0.45 mmol) in 10 mL of degassed DMF, and the pale yellow-brown solution was allowed to mix for ~20 min to ensure that all NaH had reacted. To this solution was then added a batch of (Et<sub>4</sub>N)<sub>2</sub>[NiCl<sub>4</sub>] (0.21 g, 0.44 mmol) dissolved in 2 mL of DMF. The dark red-brown solution thus obtained was stirred for 4 h at room temperature. Next, DMF was removed via short-path vacuum distillation and the residue was dissolved in 25 mL of MeCN and filtered. The resulting red solution was concentrated to ~50% of the original volume, and the desired product was isolated as a red microcrystalline solid. Yield: 0.25 g (82%). Anal. calcd for C<sub>36</sub>H<sub>52</sub>N<sub>4</sub>O<sub>2</sub>S<sub>2</sub>Ni (2): C, 62.16; H, 7.53; N, 8.05; found: 62.11; H, 7.61; N, 8.02. Selected IR bands (KBr plates, cm<sup>-1</sup>): 1521 (vs, ν<sub>co</sub>). Electronic absorption spectrum in MeCN, λ<sub>max</sub> nm (ε, M<sup>-1</sup> cm<sup>-1</sup>): 545 (sh 610), 384 (8 845), 331 (19 510). <sup>1</sup>H NMR (298 K, CD<sub>3</sub>CN, 500 MHz): (ppm from TMS) 8.06 (d, 1H), 7.95 (d, 1H), 7.22 (d, 1H), 6.78 (m, 2H), 6.51 (t, 1H), 3.14 (q, 8H), 1.11 (t, 12H).

**(Et<sub>4</sub>N)[Cu(neo)Ni(NpPepS)] (3).** A batch of 0.04 g (0.14 mmol) of [Cu(neo)Cl] was added to a red-orange solution of 0.10 g (0.14 mmol) of **1** in 10 mL of DMF. The burgundy-red homogeneous solution thus obtained was stirred for 12 h at room temperature. Next, DMF was removed in vacuo and 10 mL of MeCN was added to the residue. The pale red solution with a dark precipitate was filtered, and the dark red solid was washed with 10 mL of MeCN and dried in vacuo. Yield: 0.087 g (71%). Anal. calcd for C<sub>46</sub>H<sub>46</sub>N<sub>5</sub>O<sub>2</sub>S<sub>2</sub>CuNi (3): C, 62.27; H, 5.23; N, 7.89; found: 62.14; H, 5.31; N, 7.92. Selected IR bands (KBr plates, cm<sup>-1</sup>): 1516 (vs, ν<sub>co</sub>). Absorption spectrum in MeCN, λ<sub>max</sub> nm (ε, M<sup>-1</sup> cm<sup>-1</sup>): 495 (12 250), 420 (12 130), 326 (32 000). <sup>1</sup>H NMR (298 K, CD<sub>3</sub>CN, 500 MHz): (ppm from TMS) 8.43 (d, 1H), 7.96 (s, 1H), 7.93 (d, 1H), 7.68 (d, 1H), 7.50 (t, 2H), 7.17 (t, 1H), 6.93 (t, 1H), 6.50 (d, 1H), 6.43 (t, 1H), 3.11 (q, 4H), 2.74 (s, 3H), 1.16 (t, 6H).

**(Et<sub>4</sub>N)[Cu(neo)Ni(PhPepS)] (4).** A batch of 0.05 g (0.16 mmol) of [Cu(neo)Cl] was slowly added to a solution of 0.11 g (0.15 mmol) of **2** in 15 mL of MeCN. The deep burgundy-red solution

was then stirred at room temperature for 2 h. Next, the solvent was removed via short-path vacuum distillation and the red oily residue was triturated with 20 mL of degassed MeCN/Et<sub>2</sub>O (1:1) mixture. The red solid thus obtained was collected by filtration, washed with cold Et<sub>2</sub>O, and dried on a high-vacuum line for 1 h. Yield: 0.086 g (66%). Anal. calcd for C<sub>42</sub>H<sub>44</sub>N<sub>5</sub>O<sub>2</sub>S<sub>2</sub>CuNi (4): C, 60.25; H, 5.30; N, 8.37; found: 60.34; H, 5.23; N, 8.39. Selected IR bands (KBr plates, cm<sup>-1</sup>): 1524 (vs, ν<sub>co</sub>). Absorption spectrum in MeCN, λ<sub>max</sub> nm (ε, M<sup>-1</sup> cm<sup>-1</sup>): 495 (2 940), 363 sh (10 650), 312 sh (19 600). <sup>1</sup>H NMR (298 K, CD<sub>3</sub>CN, 500 MHz): (ppm from TMS) 8.40 (d, 1H), 8.11 (s, 1H), 7.94 (d, 1H), 7.84 (d, 1H), 7.67 (t, 1H), 6.75 (t, 1H), 6.62 (t, 1H), 6.50 (d, 1H), 6.31 (t, 1H), 3.34 (s, 3H), 3.12 (q, 4H), 1.17 (t, 6H).

**(Et<sub>4</sub>N)<sub>2</sub>[Ni{Ni(NpPepS)}<sub>2</sub>] (5).** A batch of 0.027 g of (Et<sub>4</sub>N)<sub>2</sub>[NiCl<sub>4</sub>] (0.059 mmol) dissolved in 2 mL MeCN was added to a solution containing 0.087 g (0.117 mmol) of **1** in 10 mL of degassed MeCN. The initial red-orange color of the solution turned pale orange, and a dark red microcrystalline precipitate appeared within minutes. This heterogeneous solution was stirred for 1 h, and then the mixture was filtered. The microcrystalline dark solid was collected, washed with dry Et<sub>2</sub>O, and dried in vacuo. Yield: 0.065 g (85%). Anal. calcd for C<sub>64</sub>H<sub>68</sub>N<sub>6</sub>O<sub>4</sub>S<sub>4</sub>Ni<sub>3</sub> (5): C, 59.61; H, 5.31; N, 6.52; found: 59.70; H, 5.27; N, 6.51. Selected IR bands (KBr plates, cm<sup>-1</sup>): 1538 (vs, ν<sub>co</sub>).

**(Et<sub>4</sub>N)<sub>2</sub>[Ni(DMF)<sub>2</sub>{Ni(NpPepS)}<sub>2</sub>] (6).** A batch of 0.053 g (0.04 mmol) of **5** was allowed to stir for 2 h at room temperature in 10 mL of degassed DMF. The initial heterogeneous solution slowly became homogeneous and turned bright red in color. The DMF was removed via vacuum distillation, and the resulting oily red material was triturated with 10 mL of dry Et<sub>2</sub>O to obtain the desired product as a fine red solid. Yield: 0.053 g (94%). Anal. calcd for C<sub>70</sub>H<sub>82</sub>N<sub>8</sub>O<sub>6</sub>S<sub>4</sub>Ni<sub>3</sub> (6): C, 58.56; H, 5.76; N, 7.80; found: 58.64; H, 5.73; N, 7.79. Selected IR bands (KBr plates, cm<sup>-1</sup>): 1645 (s, ν<sub>co</sub> DMF), 1532 (vs, ν<sub>co</sub>). Absorption spectrum in DMF, λ<sub>max</sub> nm (ε, M<sup>-1</sup> cm<sup>-1</sup>): 525 (sh), 437 (12 410).

**(Et<sub>4</sub>N)<sub>2</sub>[Ni{Ni(PhPepS)}<sub>2</sub>] (7).** A solution of 0.035 g of (Et<sub>4</sub>N)<sub>2</sub>[NiCl<sub>4</sub>] (0.075 mmol) dissolved in 3 mL of MeCN was added to a red-orange solution of 0.102 g (0.147 mmol) of **2** in 20 mL of degassed MeCN. The color of the reaction mixture rapidly turned to dark red. The deep red solution was stirred for 1 h at room temperature, and then its volume was reduced to half by short-path vacuum distillation. Storage of this solution at -20 °C for 16 h resulted in the precipitation of a red crystalline solid. This microcrystalline red solid was collected, washed with dry Et<sub>2</sub>O, and dried in vacuo. Yield: 0.080 g (92%). Anal. calcd for C<sub>56</sub>H<sub>64</sub>N<sub>6</sub>O<sub>4</sub>S<sub>4</sub>Ni<sub>3</sub> (7): C, 56.55; H, 5.42; N, 7.07; found: 56.64; H, 5.37; N, 7.10. Selected IR bands (KBr plates, cm<sup>-1</sup>): 3052 (w), 2983 (w), 1591 (s), 1566 (s), 1538 (vs, ν<sub>co</sub>), 1467 (s), 1442 (s), 1393 (w), 1345 (s), 1295 (w), 1268 (m), 1220 (w), 1182 (w), 1172 (w), 1140 (w), 1118 (w), 1059 (w), 1040 (w), 1002 (w), 956 (w), 791 (w), 755 (m), 691 (w), 601 (w), 515 (w). Absorption spectrum in MeCN, λ<sub>max</sub> nm (ε, M<sup>-1</sup> cm<sup>-1</sup>): 850 sh (800), 660 (2500), 560 sh (3030), 470 (3850). <sup>1</sup>H NMR (298 K, CD<sub>3</sub>CN, 500 MHz): (ppm from TMS) 8.07 (d, 1H), 7.95 (d, 1H), 7.21 (d, 1H), 6.78. (m, 2H), 6.50 (t, 1H), 3.14 (q, 4H), 1.13 (t, 6H).

**(Et<sub>4</sub>N)<sub>2</sub>[Ni(DMF)<sub>2</sub>{Ni(PhPepS)}<sub>2</sub>] (8).** A batch of 0.027 g (0.022 mmol) of **7** was allowed to stir for 2 h at room temperature in 5 mL of degassed DMF. Next, the solvent was removed via vacuum distillation and the resulting oily red material was triturated with 5 mL of dry Et<sub>2</sub>O to obtain the desired product as a fine red solid. Yield: 0.028 g (97%). Anal. calcd for C<sub>62</sub>H<sub>78</sub>N<sub>8</sub>O<sub>6</sub>S<sub>4</sub>Ni<sub>3</sub> (8): C, 55.75; H, 5.89; N, 8.39; found: 55.74; H, 5.83; N, 8.41. Selected IR bands (KBr plates, cm<sup>-1</sup>): 1646 (vs, ν<sub>co</sub> DMF), 1538 (vs, ν<sub>co</sub>).

Absorption spectrum in DMF,  $\lambda_{\text{max}}$  nm ( $\epsilon$ ,  $\text{M}^{-1} \text{cm}^{-1}$ ): 527 (1080), 380 sh (15 300), 335 (38 130).

**[Ni(terpy)Ni(NpPepS)] (9).** A slurry of 0.048 g (0.13 mmol) of  $[\text{Ni}(\text{terpy})\text{Cl}_2]$  in 1 mL of MeCN was added to a solution containing 0.100 g (0.13 mmol) of **1** in 10 mL MeCN. Within 5 min, the initial red-orange solution turned pale and a red-brown precipitate appeared. The precipitate was filtered, washed with cold MeCN, and dried in vacuo. Yield: 0.076 g (75%). Anal. calcd for  $\text{C}_{39}\text{H}_{25}\text{N}_5\text{O}_2\text{S}_2\text{Ni}_2$  (**9**): C, 60.27; H, 3.24; N, 9.01; found: 60.21; H, 3.30; N, 8.97. Selected IR bands (KBr plates,  $\text{cm}^{-1}$ ): 3051 (w), 1585 (s), 1568 (s), 1531 (vs,  $\nu_{\text{CO}}$ ), 1474 (m), 1451 (m), 1429 (w), 1385 (s), 1355 (m), 1321 (w), 1265 (w), 1248 (w), 1184 (w), 1163 (w), 1112 (w), 1095 (w), 1054 (w), 1035 (w), 1016 (w), 958 (w), 820 (w), 771 (m), 742 (m), 680 (w), 650 (w), 642 (w), 619 (w), 592 (w). Absorption spectrum in DMF,  $\lambda_{\text{max}}$  nm ( $\epsilon$ ,  $\text{M}^{-1} \text{cm}^{-1}$ ): 450 sh (8500), 427 (10 200), 337 (34 680).

**[Ni(dppe)Ni(PhPepS)] (10).** A batch of 0.154 g (0.292 mmol) of  $[\text{Ni}(\text{dppe})\text{Cl}_2]$  was slowly added to a solution of 0.204 g (0.293 mmol) of **2** in 10 mL of MeCN. Almost immediately, the red-brown solution turned pale and a blue-green microcrystalline solid appeared in the reaction mixture. The solid was filtered, washed with cold MeCN, and dried in vacuo. Yield: 0.223 g (85%). Anal. calcd for  $\text{C}_{46}\text{H}_{46}\text{N}_5\text{O}_2\text{S}_2\text{CuNi}$  (**10**): C, 61.92; H, 4.07; N, 3.14; found: 62.03; H, 4.16; N, 3.12. Selected IR bands (KBr plates,  $\text{cm}^{-1}$ ): 1538 (vs,  $\nu_{\text{CO}}$ ). Electronic absorption spectrum in  $\text{CH}_2\text{Cl}_2$ ,  $\lambda_{\text{max}}$  nm ( $\epsilon$ ,  $\text{M}^{-1} \text{cm}^{-1}$ ): 594 (3 040), 506 (sh 1 890), 345 (21 910).  $^1\text{H}$  NMR (298 K,  $\text{CDCl}_3$ , 500 MHz): (ppm from TMS) 8.03 (m, 2H), 7.90 (s, 2H), 7.61 (s, 5H), 7.39 (s, 1H), 7.31 (s, 2H), 6.96 (t, 1H), 6.74 (t, 1H), 6.51 (t, 1H), 6.43 (d, 1H), 1.87 (t, 2H).

**Physical Measurements.** Electronic absorption spectra were recorded on a Perkin-Elmer Lambda 9 UV/vis/NIR spectrophotometer. A Perkin-Elmer Spectrum One or Nicolet Nexus 870 FTIR was used to monitor the infrared spectra. The  $^1\text{H}$  NMR spectra were recorded at 298 K on a Varian Unity Plus 500 MHz spectrometer. EPR spectra were collected on a Bruker EleXsys E500 spectrometer at X-band frequencies at liquid- $\text{N}_2$  temperature. A Johnson-Matthey magnetic susceptibility balance was used to determine the room-temperature magnetic susceptibility values of the solid complexes. Electrochemical measurements were performed with Princeton Applied Research instrumentation (model 273A) at 298 K in DMF or  $\text{CH}_2\text{Cl}_2$  using either 0.1 M  $(\text{Et}_4\text{N})(\text{ClO}_4)$  or  $(n\text{Bu}_4\text{N})(\text{PF}_6)$  as the supporting electrolyte. The working electrode was a Beckman Pt-inlay working electrode, and the potentials were measured versus a SCE.

**X-ray Data Collection and Structure Solution and Refinement.** Red needles of **2** were grown by slow diffusion of  $\text{Et}_2\text{O}$  into a dilute solution of **2** in MeCN at 4 °C. Red plates of  $\mathbf{3} \cdot 0.5\text{Et}_2\text{O} \cdot 0.5\text{H}_2\text{O}$  were obtained from slow diffusion of  $\text{Et}_2\text{O}$  into a saturated solution of **3** in MeCN/DMF (1:1). Red needles of  $\mathbf{4} \cdot \text{H}_2\text{O}$  were obtained upon slow cooling of an MeCN/ $\text{Et}_2\text{O}$  (1:1) solution of the complex at -20 °C. Black blocks of  $\mathbf{5} \cdot \text{DMF}$  were obtained by slow diffusion of  $\text{Et}_2\text{O}$  into a saturated solution of the complex in MeCN/DMF (9:1). Red parallelepipeds of  $\mathbf{6} \cdot 3\text{DMF}$  were grown by diffusion of  $\text{Et}_2\text{O}$  into a dilute solution of the complex in DMF. Red blocks of **8** were grown by slow diffusion of  $\text{Et}_2\text{O}$  into a dilute solution of the complex in DMF. Black prisms of  $\mathbf{10} \cdot \text{CH}_2\text{Cl}_2$  were obtained from slow evaporation of a concentrated solution of **10** in a  $\text{CH}_2\text{Cl}_2$ /toluene (3:1) mixture at room temperature. Diffraction data for **2**,  $\mathbf{4} \cdot \text{H}_2\text{O}$ , and  $\mathbf{10} \cdot \text{CH}_2\text{Cl}_2$  were collected at 91 K on a Bruker APEX system. Diffraction data for  $\mathbf{3} \cdot 0.5\text{Et}_2\text{O} \cdot 0.5\text{H}_2\text{O}$ ,  $\mathbf{5} \cdot \text{DMF}$ , and **8** were collected at 91 K on a Bruker SMART 1000 system. For these structures, Mo  $\text{K}\alpha$  (0.71073 Å) radiation was used and the data were corrected for absorption. Diffraction data

for  $\mathbf{6} \cdot 3\text{DMF}$  were collected at 130 K on a Siemens P4 system. Cu  $\text{K}\alpha$  (1.54178 Å) radiation was used, and the data were corrected for absorption. The structures were solved using the standard SHELXS-97 package. Machine parameters, crystal data, and data collection parameters for all the complexes are summarized in Table S1, while selected bond distances and angles are reported in Table S2. Both these tables have been submitted as Supporting Information along with other crystallographic data for all of the complexes.

## Results and Discussion

**Synthesis.** The  $\text{Ni}_d$  mimics **1**<sup>26</sup> and **2**<sup>27a</sup> served as the metallosynthons in the construction of the higher-nuclearity analogues reported in this account. To date, several Ni(II)–dicarboxamido–dithiolato complexes have been reported in the literature.<sup>19,21,31–33</sup> The synthetic route that we have followed to obtain the Ni(II) complexes **1** and **2** was originally developed in this laboratory for the synthesis of Fe(III)–carboxamide complexes.<sup>34</sup> Reactions of  $(\text{Et}_4\text{N})_2[\text{NiCl}_4]$  with the deprotonated (with the aid of NaH) ligands  $\text{NpPepS}^{4-}$  or  $\text{PhPepS}^{4-}$  in solvents such as DMF readily afford complexes **1** and **2** in high yields. These Ni(II) complexes with  $\text{N}_2\text{S}_2$  chromophores are inherently stable in the solid state.

Failures in the initial attempts to synthesize Ni–Cu dinuclear model complexes in the present work provide some synthetic tips for isolation of such systems. Addition of simple Cu(I) salts such as CuCl or  $[\text{Cu}(\text{MeCN})_4]\text{PF}_6$  to DMF solutions of the  $\text{Ni}_d$  mimic **1** invariably results in the formation of the trinuclear species  $(\text{Et}_4\text{N})[\text{Cu}\{\text{Ni}(\text{NpPepS})\}_2]$  regardless of the choice of solvent, Cu(I) salt, or reagent stoichiometry.<sup>27b</sup> This observation suggests that, in order to synthesize discrete dinuclear species, one must employ Cu(I) starting complexes with less-labile ligands. Use of the trinuclear Cu(I) complex  $[\text{Cu}_3(\text{edt})_3]^{3-}$  (edt = 1,2-ethanedithiol),<sup>29b</sup> however, leads to no reaction with **1** or **2** in solvents such as DMF, MeCN, or MeOH at room temperature. When reaction mixtures with **1** is heated to 65 °C in DMF for 24 h, one obtains the trinuclear complex  $(\text{Et}_4\text{N})[\text{Cu}\{\text{Ni}(\text{NpPepS})\}_2]$  instead of the desired S-bridged Ni–Cu complex  $[\text{Cu}(\text{edt})\text{Ni}(\text{NpPepS})]^{3-}$ . In contrast, when one employs  $[\text{Cu}(\text{neo})(\text{Cl})]^{29a}$  as the starting Cu(I) complex, the reaction indeed takes the desired course. For instance, reaction of  $[\text{Cu}(\text{neo})\text{Cl}]$  with **1** or **2** in MeCN at room temperature cleanly affords the Ni–Cu dinuclear complexes **3** and **4**, respectively, in high yields. Clearly, the strong preference of the neo ligand for Cu(I) center, as well as the tetrahedral geometric preference of Cu(I), allows for the formation of **3** and **4**. Complexes **3** and **4** are also obtained when  $[\text{Cu}(\text{neo})(\text{SR})]$  ( $\text{R} = \text{C}_6\text{H}_5$ ,  $p\text{-C}_6\text{H}_4\text{-Cl}$ )<sup>29c</sup> are used as the starting Cu(I) complexes. In the solid state, **3** and **4** are stable for months and no oxidation of the Cu(I) center is observed (as verified by  $^1\text{H}$  NMR and electronic absorption spectroscopy).

(31) (a) Krüger, H.-J.; Peng, G.; Holm, R. H. *Inorg. Chem.* **1991**, 30, 734–742. (b) Krüger, H.-J.; Holm, R. H. *Inorg. Chem.* **1987**, 26, 3645–3647.

(32) Dutton, J. C.; Fallon, G. D.; Murray, K. S. *Chem. Lett.* **1990**, 983–986.

(33) Hanss, J.; Krüger, H.-J. *Angew. Chem., Int. Ed.* **1998**, 37, 360–363.

(34) Marlin, D. S.; Mascharak, P. K. *Chem. Soc. Rev.* **2000**, 29, 69–74.

Similar reactivity has also been noted in our attempts to synthesize dinuclear Ni(II) species. Reactions of Ni(II) salts such as  $(\text{Et}_4\text{N})_2[\text{NiCl}_4]$  with **1** or **2** in MeCN afford the corresponding trinuclear complexes **5** and **7** in high yield. These trinuclear complexes form regardless of the Ni(II) salt/metallosynthon stoichiometry. Isolation of these complexes is aided by the high insolubility of **5** and **7** in MeCN; the trinuclear complexes precipitate out of solution within minutes. Interestingly, dissolution of **5** and **7** in DMF (a slow process) results in coordination of two molecules of DMF to the central Ni(II) ion (designated as  $\text{Ni}_\text{C}$ ) affording the DMF adducts **6** and **8**, respectively. This binding is also reversible. When the DMF adducts **6** and **8** are treated with solvents such as MeCN or THF, the respective trinuclear species **5** and **7** form almost immediately (verified by IR and  $^1\text{H}$  NMR).

The dinuclear Ni–Ni model complexes have been synthesized by following the strategy used to isolate the Ni–Cu complexes **3** and **4**. Reaction of 1 equiv of  $[\text{Ni}(\text{terpy})\text{Cl}_2]$  (terpy = 2,2':6',2''-terpyridine) with **1** in MeCN affords **9**, a Ni–Ni dimer in which the modeled  $\text{Ni}_\text{p}$  site is five-coordinate. The isolation of **9** is aided by its lack of solubility in a variety of polar solvents such as MeOH and MeCN due to the overall neutral charge of the complex. Since the as-isolated  $\text{Ni}_\text{p}$  site of ACS is four-coordinate in the crystal structure, we employed a second  $\text{Ni}_\text{p}$  synthon,  $[\text{Ni}(\text{dppe})\text{Cl}_2]$  (dppe = 1,2-bis(diphenylphosphino)ethane), in such reaction. This  $\text{Ni}_\text{p}$  synthon is expected to favor an easier reduction to the Ni(I) oxidation state and further facilitate binding of CO. However, all attempts to synthesize a Ni–Ni dimer with **1** and  $[\text{Ni}(\text{dppe})\text{Cl}_2]$  led to the formation of the trinuclear species **5**. In contrast, reaction of **2** with 1 equiv of  $[\text{Ni}(\text{dppe})\text{Cl}_2]$  in MeCN affords **10** as a blue-green microcrystalline solid in 85% yield. Steric interactions between the folded structure of the  $\{\text{Ni}(\text{NpPepS})\}$  moiety<sup>26</sup> and the dppe ligand frame presumably prevent the formation of the dinuclear complex in the first case, while the more rigid ligand frame of **2** allows formation of the desired dimer **10** without such hindrance. It is therefore evident that proper design of the ligand frame of the  $\text{Ni}_\text{d}$  metallosynthon is crucial for the successful isolation of  $\text{Ni}_\text{p}$ – $\text{Ni}_\text{d}$  ACS models.

**Structure and Properties.  $(\text{Et}_4\text{N})_2[\text{Ni}(\text{PhPepS})]$  (**2**).** The structure of  $[\text{Ni}(\text{PhPepS})]^{2-}$  (anion of **2**) is shown in Figure 3. The coordination geometry around nickel is square planar arising from two carboxamido nitrogens and two thiolato sulfurs in cis geometry. Although the overall disposition of the  $\text{PhPepS}^{4-}$  ligand frame is similar to that of  $\text{NpPepS}^{4-}$  in **1**,<sup>26</sup> there are some noted differences. For example, the extent of the ‘butterfly’ folding of the aryl sulfur rings observed in **1** is not as extreme in the case of **2**. This is reflected in the more rigid five-member chelate ring of the phenylenediamido portion of **2** (nearly coplanar with the  $\text{NiN}_2\text{S}_2$  plane) compared to the six-member chelate ring of the naphthalenediamido portion of **1** (almost perpendicular to the  $\text{NiN}_2\text{S}_2$  plane). Interestingly,  $[\text{Ni}(\text{tsalphen})]$ , an analogous Ni(II) complex derived from a ligand frame similar to **2** but with imine nitrogen coordination, is completely planar.<sup>35</sup> This suggests that the bending of the aryl rings is most likely due

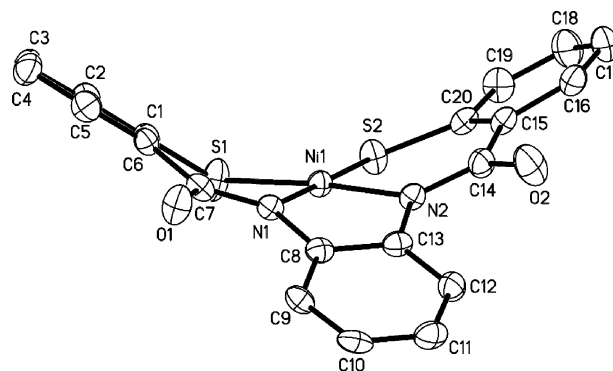


**Figure 3.** ORTEP diagram of the anion  $[\text{Ni}(\text{PhPepS})]^{2-}$  (anion of **2**) (50% probability) with the atom-labeling scheme. H atoms are omitted for the sake of clarity.

to the presence of the carboxamido nitrogens in **2**. The angles at the Ni(II) center are slightly distorted from the ideal  $90^\circ$  value due to the short bite of the phenylenediamido portion of the ligand frame ( $\text{N1–Ni–N2} = 85.52(11)^\circ$ ). The average  $\text{Ni–N}_{\text{amido}}$  bond length ( $1.907(3)$  Å) compares well with other Ni(II)–carboxamido complexes.<sup>21,26,31–33,36</sup> The average  $\text{Ni–S}$  bond distance ( $2.158(10)$  Å) is also within the range of Ni–S distances found in analogous Ni(II)–dicarboxamido–dithiolato species.<sup>21,26,31–33</sup>

Coordination of deprotonated carboxamido nitrogen to metal centers is readily indicated by the red-shift of the carbonyl stretching frequency ( $\nu_{\text{co}}$ ) of the complex with respect to the  $\nu_{\text{co}}$  of the free ligand.<sup>34</sup> Complex **2** exhibits its  $\nu_{\text{co}}$  at  $1521\text{ cm}^{-1}$  compared to  $1652\text{ cm}^{-1}$  for the free ligand  $\text{PhPepSH}_4$ . In MeCN, **2** exhibits a dark red color arising from strong ligand-to-metal charge-transfer absorption at 384 nm and a d–d band at 545 nm typical for Ni(II) complexes with dicarboxamido–dithiolato ( $\text{N}_2\text{S}_2$ ) coordination.<sup>21,26,31–33</sup> The clean  $^1\text{H}$  NMR spectrum of **2** in  $\text{CD}_3\text{CN}$  confirms that the square-planar geometry of **2** is retained in solution. Ligation of deprotonated carboxamido nitrogen to nickel in general provides exceptional stability to the 2+ and 3+ oxidation states.<sup>21,31–33</sup> In DMF, **2** displays an irreversible metal-centered oxidation wave at 0.22 V (vs SCE). This value is more positive than the oxidation potential of other Ni(II)– $\text{N}_2\text{S}_2$  complexes possibly due to the weaker donor strength of the aryl thiolate donors in **2** compared to the alkanethiolates present in analogous complexes. Not surprisingly, **2** exhibits no reduction wave down to a potential of  $-1.8$  V (vs SCE, DMF) due to the presence of strong  $\sigma$ -donors (carboxamido-N and thiolato-S) around the Ni(II) center.

**$(\text{Et}_4\text{N})[\text{Cu}(\text{neo})\text{Ni}(\text{NpPepS})]$  (**3**).** The structure of **3** consists of a square-planar Ni(II) ion bridged to a distorted tetrahedral Cu(I) center via the thiolato-S donors of the  $\text{NpPepS}^{4-}$  ligand frame (Figure 4). Close scrutiny of the  $\text{Ni–N}_{\text{amido}}$  and  $\text{Ni–S}$  bond distances in **3** (av =  $1.899(4)$  and  $2.1950(15)$  Å, respectively) reveals little changes from those noted for the Ni(II) monomer **1**. The  $\text{Cu}\cdots\text{Ni}$  distance of **3** ( $3.074$  Å) is somewhat longer than that of the Cu form of ACS/CODH ( $2.792$  Å).<sup>5</sup> Steric constraints imposed by the

(35) Smeets, W. J. J.; Spek, A. L.; Henderson, R. K.; Bouwman, E.; Reedijk, J. *Acta Crystallogr., Sect. C* **1997**, *C53*, 1564–1566.



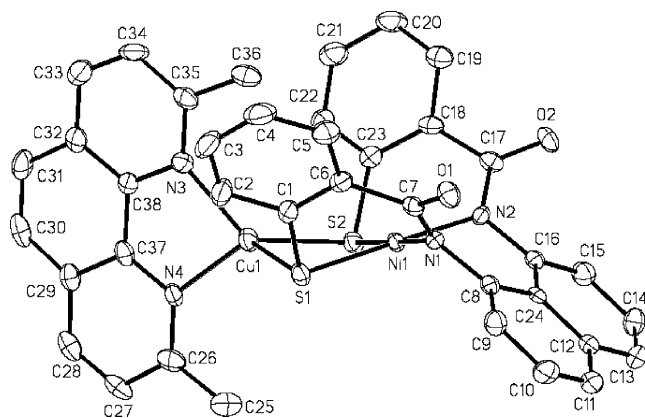


**Figure 4.** ORTEP diagram of  $[\text{Cu}(\text{neo})\text{Ni}(\text{NpPepS})]^-$  (anion of **3**) (50% probability) with the atom-labeling scheme. H atoms are omitted for the sake of clarity.

$\text{NpPepS}^{4-}$  ligand frame are presumably responsible for the longer metal–metal distance compared with the enzyme value. The average Cu–N distance in **3** (2.047(4) Å) is typical of Cu(I)–neocuproine-type complexes.<sup>37</sup> However, the two Cu–S distances are quite different with Cu–S1 = 2.2670(16) and Cu–S2 = 2.3198(16) Å. The distorted arrangement of the donor atoms around the Cu(I) center is further supported in the large deviation of the bond angles (N3–Cu–N4 = 82.66(18)° and N3–Cu–S1 = 129.79(14)°) from the ideal tetrahedral value of 109.5°. Similar distortion has also been observed in other sulfur-bridged Ni(II)–Cu(I) complexes.<sup>25,27b</sup>

Metalation of the sulfur ligands of the  $\{\text{Ni}(\text{NpPepS})\}$  moiety in **3** is readily indicated by the blue-shift of the  $\nu_{\text{co}}$  value of the complex (1516  $\text{cm}^{-1}$  compared to 1510  $\text{cm}^{-1}$  in monomeric **1**). Enhanced charge donation by the carboxamido-N to compensate for the decreased donor strength of sulfur (following metalation by Cu) is presumably responsible for this blue-shift. Complex **3** is diamagnetic and exhibits a clean  $^1\text{H}$  NMR spectrum. Although metalation of thiolate-S donors can alter the charge density at the Ni(II) center making the Ni(I) oxidation state more accessible,<sup>23</sup> **3** does not exhibit any observable redox wave down to –1.8 V (vs SCE, DMF). Clearly, the Ni(I) state is not supported in this complex even with sulfur metalation. This lends further support toward a nonredox role for the  $\text{Ni}_d$  site in the enzyme.

**(Et<sub>4</sub>N)[Cu(neo)Ni(PhPepS)] (4).** The structure of the anion of the dinuclear Ni(II)–Cu(I) complex **4** is shown in Figure 5. Much like **3**, this complex also consists of a square-planar Ni(II) ion sulfur-bridged to a distorted tetrahedral Cu(I) center. The metric parameters of the  $\text{NiN}_2\text{S}_2$  portion of **4** (av Ni–N<sub>amido</sub> = 1.9037(11) Å) are similar to that of monomer **2** except for slight elongation of the Ni–S bond distance (av = 2.1872(4) Å). Also, the bending of the aryl thiolate rings away from the  $\text{NiN}_2\text{S}_2$  coordination plane is more noticeable in **4** compared to **2** as a result of the steric clash between the methyl groups of the neocuproine unit with the  $\text{PhPepS}^{4-}$  ligand frame. This is reflected in the change

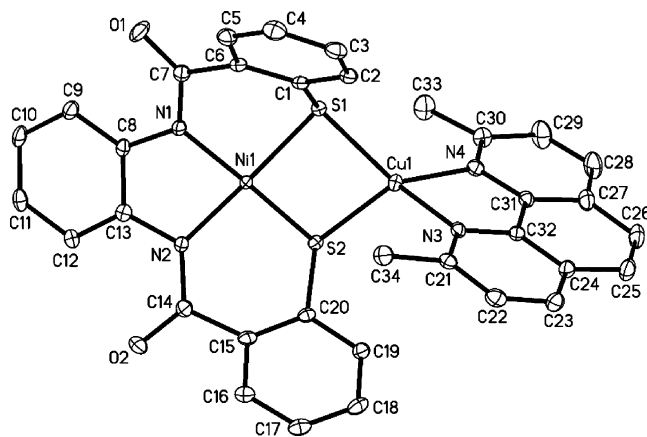


**Figure 5.** ORTEP diagram of  $[\text{Cu}(\text{neo})\text{Ni}(\text{PhPepS})]^-$  (anion of **4**) (50% probability) with the atom-labeling scheme. H atoms are omitted for the sake of clarity.

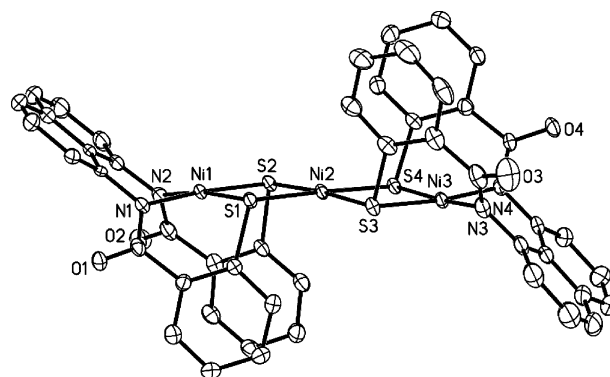


**Figure 6.** ORTEP diagram of  $[\text{Ni}\{\text{Ni}(\text{NpPepS})\}_2]^{2-}$  (anion of **5**) (50% probability) with the atom-labeling scheme. H atoms are omitted for the sake of clarity.

of the C1–S1–Ni angle which is more compressed in **4** (99.06(5)°) than in **2** (106.53(11)°) and the highly distorted tetrahedral geometry about the Cu(I) center. For example, there is a significant difference in the two Cu–N bond lengths (Cu–N3 = 2.0194(14) Å; Cu–N4 = 2.0894(14) Å), the two Cu–S distances (Cu–S1 = 2.2496(4) Å; Cu–S2 = 2.3508(4) Å), and the bond angles range from 82.08(5)° (N3–Cu–N4) to 140.13(4)° (N3–Cu–S1). As a result, the Cu···Ni bond distance of **4** (3.1435(2) Å) is longer than that observed in Cu–ACS. Like **3**, complex **4** exhibits a clean diamagnetic  $^1\text{H}$  NMR spectrum and exhibits no Ni(II)/Ni(I) reduction wave in its cyclic voltammogram.

**(Et<sub>4</sub>N)<sub>2</sub>[Ni{Ni(NpPepS)}<sub>2</sub>] (5).** An ORTEP drawing of the anion of the trinuclear Ni(II) complex **5** is shown in Figure 6. The two terminal Ni(II) centers (designated as  $\text{Ni}_T$ ; Ni1 and Ni3 in Figure 5) and the central Ni(II) center (designated as  $\text{Ni}_C$ ; Ni2 in Figure 5) of **5** all lie in one extended plane in a slant chair configuration resulting from the orientation of the naphthalene rings. The two aryl sulfur rings of the  $\text{NpPepS}^{4-}$  ligand frame fold in an up–down sequence and appear as railings for the  $\text{N}_2\text{Ni}_T\text{S}_2$ – $\text{Ni}_C$ – $\text{S}_2$ – $\text{Ni}_T\text{N}_2$  platform. The  $\text{Ni}_T$ –N<sub>amido</sub> and  $\text{Ni}_T$ –S bond distances in **5** (av = 1.880(3) and 2.1769 Å, respectively) are similar to those observed in **1**, while the average  $\text{Ni}_C$ –S bond length (2.2368(10) Å) is slightly longer than those distances observed in similar Ni(II) trinuclear species.<sup>21,38</sup> Unique

(36) Chapman, R. L.; Vagg, R. S. *Inorg. Chim. Acta* **1979**, *33*, 227–234.

(37) Pallenberg, A. J.; Koenig, K. S.; Barnhart, D. M. *Inorg. Chem.* **1995**, *34*, 2833–2840.

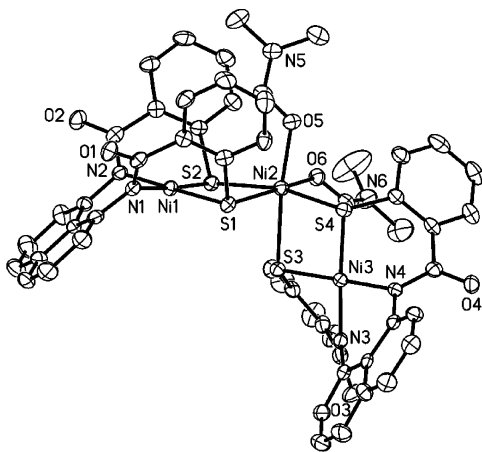


**Figure 7.** ORTEP diagram of  $[\text{Ni}(\text{DMF})_2\{\text{Ni}(\text{NpPepS})\}_2]^{2-}$  (anion of **6**) (50% probability) with the atom-labeling scheme. H atoms are omitted for the sake of clarity.

folding of the  $\text{NpPepS}^{4-}$  ligand around the  $\text{Ni}_\text{T}$  centers in **5** is presumably responsible for this lengthening of the  $\text{Ni}_\text{C}$ –S bonds. Further comparison of the structural parameters of **5** with those of **1** reveal several differences in the coordination structure and ligand folding about the  $\text{Ni}(\text{II})$  centers. For example, in **5**, the  $\text{S1}–\text{Ni1}–\text{S2}$  bite angle is more compressed ( $86.85(4)^\circ$ ) compared to **1** ( $91.91(10)^\circ$ ) as a result of  $\text{Ni}_\text{C}$  coordination. Most notably, the ‘butterfly’ folding of the aryl sulfur rings in **5** allow the two adjacent rings on each  $\text{NpPepS}^{4-}$  ligand frame to become much closer to each other compared to **1**. Finally, the  $\text{C1}–\text{S1}–\text{Ni1}$  bond angle is considerably more closed in **5** ( $87.72(13)^\circ$ ) than in **1** ( $101.2(2)^\circ$ ).

The extremely low solubility of **5** in  $\text{CD}_3\text{OD}$ ,  $\text{CD}_3\text{CN}$ , and  $\text{CD}_2\text{Cl}_2$  prevented the recording of its  $^1\text{H}$  NMR spectrum, although magnetic moment measurement (polycrystalline sample) confirmed its  $S = 0$  spin state. As discussed below, dissolution of **5** in deuterated DMF or DMSO affords paramagnetic species due to solvent binding to  $\text{Ni}_\text{C}$  and such solutions exhibit broad NMR signals. Metalation of the sulfurs in **5** was also confirmed by the blue-shift of its  $\nu_{\text{co}}$  band ( $1538\text{ cm}^{-1}$ ) compared to **1** ( $1510\text{ cm}^{-1}$ ).

**(Et<sub>4</sub>N)<sub>2</sub>[Ni(DMF)<sub>2</sub>{Ni(NpPepS)}<sub>2</sub>] (6).** The structure of the anion of the DMF adduct **6** is shown in Figure 7. The binding of two molecules of DMF to  $\text{Ni}_\text{C}$  in **5** results in significant structural rearrangement. Major rearrangement occurs to accommodate the two additional DMF ligands coordinated to the  $\text{Ni}_\text{C}$  center in cis fashion by rotation of one of the  $\text{Ni}_\text{T}\text{N}_2\text{S}_2$  units by  $\sim 90^\circ$  to afford a distorted octahedral coordination unit around  $\text{Ni}_\text{C}$ . Although the average  $\text{Ni}–\text{N}_{\text{amido}}$  and  $\text{Ni}–\text{S}$  bond lengths of the  $\text{Ni}_\text{T}$  sites in **6** ( $1.893(3)$  and  $2.1758(12)\text{ Å}$ , respectively) remain unchanged (compared to **1** and **5**), the  $\text{Ni}_\text{C}–\text{S}$  bond distances ( $\text{av} = 2.4447(12)\text{ Å}$ ) increase significantly compared with **5** ( $\text{av} = 2.2368(10)\text{ Å}$ ) upon expansion of the coordination sphere. Additionally, this results in a longer  $\text{Ni}\cdots\text{Ni}$  separa-

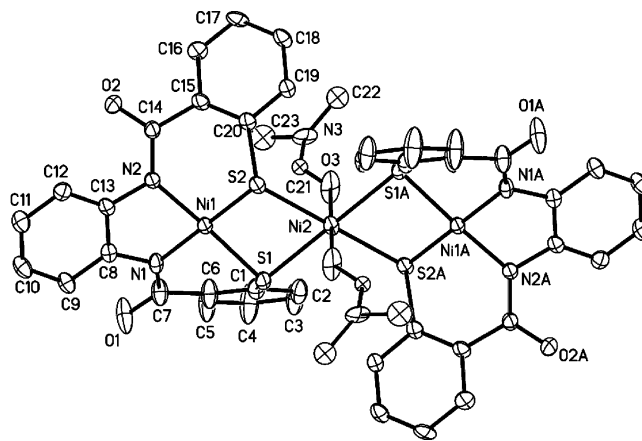


**Figure 8.** ORTEP diagram of  $[\text{Ni}(\text{DMF})_2\{\text{Ni}(\text{PhPepS})\}_2]^{2-}$  (anion of **8**) (50% probability) with the atom-labeling scheme. H atoms are omitted for the sake of clarity.

tion in **6** ( $3.374\text{ Å}$ ) compared to **5** ( $3.2269(7)\text{ Å}$ ). The bending of the aryl sulfur rings of the  $\text{Ni}_\text{T}\text{N}_2\text{S}_2$  units in **6** is also less pronounced ( $\text{C1}–\text{S1}–\text{Ni1} = 97.67(14)^\circ$  compared to  $87.72(13)^\circ$  in **5**). A small trans influence of the coordinated DMF molecules in **6** is reflected in the two longer  $\text{Ni}_\text{C}–\text{S}$  bond distances ( $\text{Ni2}–\text{S1} = 2.4877(13)\text{ Å}$ ;  $\text{Ni2}–\text{S3} = 2.4495(12)\text{ Å}$ ). The increase in  $\text{Ni}_\text{C}–\text{S}$  could also arise from the increased metal–ligand electron repulsion in going from low-spin planar **5** ( $S = 0$ ) to high-spin octahedral **6** ( $S = 1$ ).

Complex **6** exhibits an additional  $\nu_{\text{co}}$  stretch at  $1645\text{ cm}^{-1}$  due to the O-coordinated DMF molecules at the  $\text{Ni}_\text{C}$  center. The  $S = 1$  spin state of **6** has been confirmed by measurement of the magnetic moment of the complex in the polycrystalline state ( $\mu_{\text{eff}} = 2.87\text{ } \mu_{\text{B}}$  at  $298\text{ K}$ ).

**(Et<sub>4</sub>N)<sub>2</sub>[Ni{Ni(PhPepS)}<sub>2</sub>] (7).** So far, we have not been able to grow good quality crystals of this complex for diffraction studies. However, microanalytical and spectroscopic data confirm an extended planar structure similar to that of complex **5**. This diamagnetic complex is more soluble in a variety of solvents than its analogue **5**, and its clean  $^1\text{H}$  NMR spectrum in  $\text{CD}_3\text{CN}$  is consistent with square-planar coordination around the three  $\text{Ni}(\text{II})$  centers. The electronic absorption spectrum of **7** consists of several peaks in the  $400–500\text{ nm}$  range arising from multiple ligand-to-metal charge transfer (LMCT) bands arising from the  $\text{NiS}_4$  and  $\text{NiN}_2\text{S}_2$  chromophores. As expected, the  $\nu_{\text{co}}$  band of **7** is shifted to higher energy ( $1538\text{ cm}^{-1}$ ) compared to the monomeric complex **2** ( $1521\text{ cm}^{-1}$ ).

**(Et<sub>4</sub>N)<sub>2</sub>[Ni(DMF)<sub>2</sub>{Ni(PhPepS)}<sub>2</sub>] (8).** The structure of the anion of the trinuclear complex **8** is shown in Figure 8. Much like the analogous trimer **6**, complex **8** also comprises two  $\text{Ni}_\text{T}\text{N}_2\text{S}_2$  units coordinated to an octahedral  $\text{Ni}_\text{C}$  center ( $\text{Ni2}$  in Figure 8). However, the  $\text{Ni}_\text{T}\text{N}_2\text{S}_2$  moieties prefer to stay coplanar due to the decreased steric demands of the  $\text{PhPepS}^{4-}$  ligand frame in **8**. This results in coordination of the two DMF molecules in a trans position at the  $\text{Ni}_\text{C}$  center. The average  $\text{Ni}_\text{C}–\text{S}$  and  $\text{Ni}_\text{C}–\text{O}$  bond distances of **8** ( $2.4475(16)$  and  $2.063(5)\text{ Å}$ , respectively) are very similar to those observed in **6** and other related complexes. When compared with **2**, the overall folding and metric parameters of the  $\text{PhPepS}^{4-}$  ligand frame in **8** appear relatively unchanged with

(38) (a) Farmer, P. J.; Solouki, T.; Mills, D. K.; Soma, T.; Russell, D. H.; Reibenspies, J. H.; Darensbourg, M. Y. *J. Am. Chem. Soc.* **1992**, *114*, 4601–4605. (b) Turner, M. A.; Driessen, W. L.; Reedijk, J. *Inorg. Chem.* **1990**, *29*, 3331–3335.



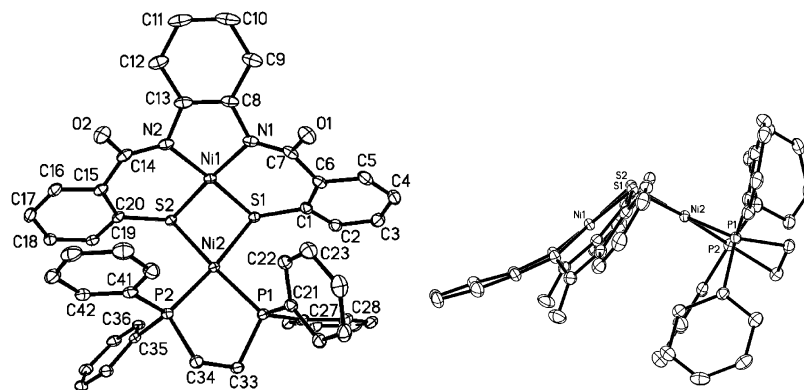


**Figure 9.** ORTEP diagram of [Ni(dppe)Ni(PhPepS)] (**10**) (50% probability) with the atom-labeling scheme (left). H atoms are omitted for the sake of clarity. A different view is shown on left showing the dihedral angle between the NiN<sub>2</sub>S<sub>2</sub> and NiS<sub>2</sub>P<sub>2</sub> plane.

only a slight increase in the Ni<sub>T</sub>–S bond length (av = 2.1723(18) Å) presumably due to metalation of sulfur by Ni<sub>C</sub>. Collectively, the structures of **6** and **8** demonstrate that minor changes in the ligand design can alter the binding mode (e.g., *cis* vs *trans* coordination) of ligands and reactivity of metal centers in these model complexes. Complex **8** displays a strong  $\nu_{\text{CO}}$  band at 1646 cm<sup>−1</sup> due to the O-coordinated DMF ligands and its magnetic moment value ( $\mu_{\text{eff}}$  = 2.89  $\mu_{\text{B}}$  at 298 K, polycrystalline sample) is consistent with an *S* = 1 ground state.

**[Ni(terpy)Ni(NpPepS)] (9).** Although we have not completed structural studies on this model complex due to lack of suitable crystals, it has been thoroughly characterized by various spectroscopic techniques and its composition has been confirmed by microanalytical data. The blue-shift in the  $\nu_{\text{CO}}$  band of complex **9** (1531 cm<sup>−1</sup>) strongly supports the proposed dinuclear structure, and the ESI-MS data support the presence of a [Ni(terpy)]<sup>2+</sup> moiety bound to a [Ni(NpPepS)]<sup>2−</sup> unit. Additional support for a five-coordinate Ni(II) center in **9** comes from the magnetic susceptibility studies ( $\mu_{\text{eff}}$  = 3.02  $\mu_{\text{B}}$  at 298 K, polycrystalline sample). Since **9** exhibits an irreversible reduction at −1.13 V (vs SCE) in DMF, it is evident that the Ni(I) state is accessible in this model complex. Although the potential is still outside the biological range, this property of **9** allows one the opportunity to study the possibility of CO binding in the reduced state (A<sub>red</sub>–CO mimic). The results of such studies are discussed in detail in a forthcoming section.

**[Ni(dppe)Ni(PhPepS)] (10).** The structure of the neutral dinuclear complex **10** is shown in Figure 9. In this Ni–Ni model, the two Ni(II) centers are connected via the two thiolato-S donors of the PhPepS<sup>4−</sup> ligand frame and both Ni centers exist in square-planar geometry. The spatial arrangement of the donor atoms of the NiN<sub>2</sub>S<sub>2</sub> portion of this complex does not change significantly from that in the monomeric complex **2**, and hence, similar Ni–N<sub>amido</sub> and Ni–S bond distances (av = 1.890(17) and 2.150(5) Å, respectively) are noted for **10**. The dihedral angle between the two Ni(II) square planes in **10** is 111.4° and the Ni⋯Ni separation is 2.8255(4) Å (Ni⋯Ni in ACS/CODH = 3.00 Å).<sup>6</sup> Coordination of the Ni<sub>p</sub> mimic to the two S-donors of the PhPepS<sup>4−</sup> results in a decrease bend of the aryl thiolate rings due to the shorter bite angle of the *cis*-dithiolato portion

of the ligand frame (S1–Ni1–S2 = 79.29(2)°). The bond angles about the bridged Ni<sub>p</sub> center (Ni2 in Figure 9) in **10** also deviate from the ideal value (P1–Ni2–P2 = 86.18(2)°; P1–Ni2–S1 = 99.13(2)°) due to steric constraints imposed by the four phenyl groups of the diphosphine ligand. The average Ni–S and Ni–P bond distances of the Ni<sub>p</sub> site in **10** (2.2384(6) and 2.1799(6) Å, respectively) are similar to those found in other dinuclear Ni complexes with P<sub>2</sub>S<sub>2</sub> coordination spheres.<sup>19,22</sup>

The dinuclear structure of **10** is readily identified by the blue-shift of the  $\nu_{\text{CO}}$  to 1538 cm<sup>−1</sup> from 1521 cm<sup>−1</sup> in the case of **2**. The two square-planar Ni(II) centers of **10** give rise to a diamagnetic species that exhibits a clean <sup>1</sup>H NMR spectrum in CDCl<sub>3</sub>.

**Reactivity with 1,10-Phenanthroline.** In some of the earliest studies on ACS/CODH (before any structural analysis), Lindahl and co-workers showed that a portion of the Ni at the A-cluster site is labile and easily removed with the bidentate chelator phen.<sup>11b</sup> This removal of “labile Ni” by phen completely inhibits the ACS activity but leaves the CODH activity intact. The phen-treated enzyme also displays no NiFeC EPR signal. We were therefore curious to determine whether the sulfur-bridged Ni in the model complexes such as **6**, **8**, and **10** can be removed with phen. Previous studies on a trinuclear model complex reported by Darensbourg and co-workers, namely [(BME-DACO)-Ni]<sub>2</sub>NiBr<sub>2</sub>, have shown that the Ni(II) center coordinated by four metallosulfur moieties from the NiN<sub>2</sub>S<sub>2</sub> units in the complex is indeed removed by phen.<sup>23</sup> However, the absence of key carboxamido groups in the NiN<sub>2</sub>S<sub>2</sub> fragments in these trinuclear species, as well as the lack of phen reactivity with a trinuclear complex similar to **6** (and **8**) with carboxamido coordination synthesized by Hegg and co-workers<sup>21</sup> prompted us to study the phen reactivity with our complexes.

Titration of solutions of **6** or **8** in DMF with phen results in immediate removal of the central Ni (Ni<sub>C</sub>) ions in both these trinuclear species. The reaction can be followed by monitoring the electronic absorption spectrum. As shown in Figure 10, the spectrum completely stops changing only after addition of 3 mol equiv of phen to **6**, suggesting formation of [Ni(phen)<sub>3</sub>]<sup>2+</sup> and 2 mol equiv of the monomer **1**.<sup>27b</sup> Similar results were obtained with complex **8**. Since no further change is observed upon addition of a large excess

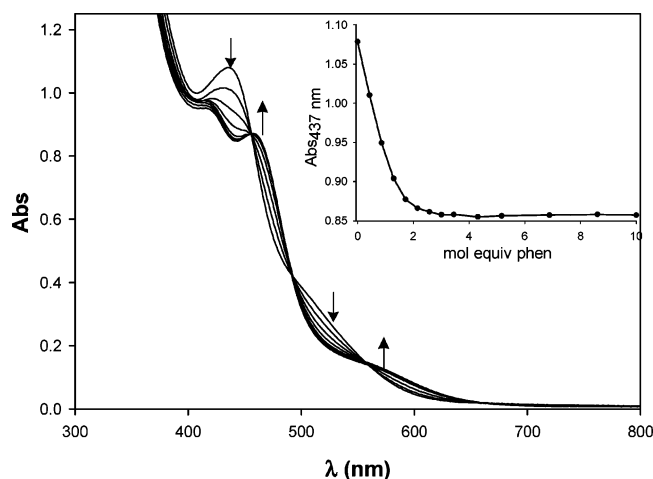


**Figure 10.** Changes in the electronic absorption spectrum of  $(\text{Et}_4\text{N})_2[\text{Ni}(\text{DMF})_2\{\text{Ni}(\text{NpPepS})\}_2]$  (**6**, 0.087 mM) upon addition of 0.5 mol equiv aliquots of phen in DMF. Inset: change in absorbance at 437 nm vs mol equiv of phen.

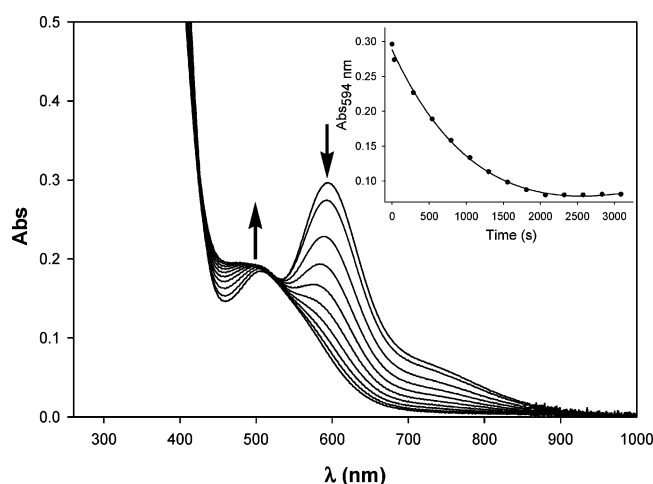


**Figure 11.** Changes in the electronic absorption spectrum of  $[\text{Ni}(\text{dppe})\text{Ni}(\text{PhPepS})]$  (**10**, 0.0974 mM) upon mixing with excess phen (25 mol equiv) in  $\text{CH}_2\text{Cl}_2$  at 298 K. Inset: change in absorbance at 594 nm vs time (s).

(~100 mol equiv) of phen to these solutions, it is evident that the Ni(II) centers in the  $\text{Ni}_d$  mimics **1** and **2** are strongly coordinated to their dicarboxamido–dithiolato ligand frames and are resistant to removal by phen.

The reactivity of phen with the dinuclear model **10** is slightly different from its trinuclear counterparts **6** and **8**.<sup>27a</sup> Addition of phen to a solution of **10** in  $\text{CH}_2\text{Cl}_2$  does remove the sulfur-bridged  $\text{Ni}_p$  model site in this complex resulting in the formation of **2**,  $[\text{Ni}(\text{phen})_3]^{2+}$ , and free dppe in solution. However, the removal of  $\text{Ni}_p$  in **10** requires excess phen (~25 mol equiv) and takes nearly 35 min to reach the end point (beyond which no further change occurs in the electronic absorption spectrum, Figure 11). The observed pseudo-first-order rate constant ( $k_{\text{obs}}$ ) for the phen removal of  $\text{Ni}_p$  in dimer **10** is  $1.50 \times 10^{-4} \text{ s}^{-1}$ . The slower phen reactivity of **10** compared to that of **6** and **8** presumably arises from the more stable square-planar low-spin nature of the  $\text{Ni}_p$  site in **10** as opposed to the high-spin octahedral  $\text{Ni}_c$  centers in **6** and **8**. Interestingly, treatment of the Ni–Cu dimers **3** and **4** with phen does not result in any reaction. However, addition of the Cu(I)-specific chelator neo to **3**

and **4** affords the respective monomers **1** and **2** and  $[\text{Cu}(\text{neo})_2]^+$ . Neocuproine exhibits no reaction with the Ni centers of **6**, **8**, or **10**. Collectively, the phen reactivity of the Ni complexes **6**, **8**, and **10** lends further support to the notion that the “labile Ni” in the enzyme originates from the  $\text{M}_p$  site and *not* the  $\text{Ni}_d$  site.<sup>11,12</sup> The results also provide indirect evidence in favor of Ni at the  $\text{M}_p$  site of the A-cluster of catalytically active ACS/CODH.

**Reactivity of Ni–Cu Models.** The Cu(I) sites in all the synthetic models reported so far exhibit no affinity toward CO. For example, the dinuclear models synthesized by Riordan and co-workers undergo rupture of the  $(\mu\text{-SR})_2$  bridge and breakdown of the dinuclear structure upon reaction with CO.<sup>25</sup> The Ni–Cu dinuclear complex,  $[\{\text{P}(\text{Pr})_3\text{Cu}\}\{\text{NiS}_2\text{N}'_2\}]^-$ , synthesized by Rauchfuss and co-workers with a coordinatively unsaturated Cu(I) center, does not exhibit any CO binding.<sup>24</sup> Although some of these models utilize Ni(II)–diamino–dithiolato complexes as the  $\text{Ni}_d$  synthon and hence lack crucial Ni(II)–carboxamido–N interaction(s),<sup>25</sup> the consistent inertness of the Cu(I) centers in these model complexes indicates a noncatalytic role for Cu in ACS/CODH.

The Ni–Cu models of the present work, namely **3** and **4**, consist of  $\text{Ni}_d$  synthons that include carboxamido ligation to the Ni(II) center. Both these models exhibit no CO binding to either metal center nor is any breakdown of the  $\text{Cu}-(\mu\text{-SR})_2\text{-Ni}$  core observed upon passage of CO through the solutions of these complexes. No breakdown of the  $\text{Cu}-(\mu\text{-SR})_2\text{-Ni}$  core is observed upon treatment with excess phen either. Clearly, the dinuclear structures are very stable and are in accord with results of previous experiments showing Cu(I) ion as a stronger binder to metallosulfur donors compared to Ni(II) and Zn(II) ions.<sup>23</sup> Although the lack of reactivity of the Cu(I) centers of **3** and **4** toward CO could simply arise from coordinative saturation (both tetrahedrally coordinated), it is important to note that exposure to CO does not cause any break in the Cu–S bridge to provide a binding site for CO. This indicates that Cu(I) binds the thiolato sulfurs of the  $\text{Ni}_d$  site quite strongly, and hence, the presence of Cu at the  $\text{M}_p$  site in Drennan’s structure could be a consequence of binding of adventitious metal ions present in the crystallization buffers.<sup>11</sup> Indeed, in a recent paper, Darensbourg and co-workers have examined the metal ion affinity of an analogous  $\text{NiN}_2\text{S}_2$  thiolato complex,  $([\text{BME-DACO}]\text{Ni})$ , and the results indicate that the affinity decreases in the order  $\text{Cu(I)} > \text{Ni(II)} > \text{Zn(II)}$ .<sup>23</sup>

**Reactivity of Ni–Ni Models.** Since one of the steps of the proposed ACS mechanism invokes the formation of a Ni(I)–CO species responsible for the NiFeC EPR signal, we have studied the redox properties and CO affinities of the bridged Ni(II) centers in **6** and **8**–**10**. The redox behaviors of the models of the  $\text{Ni}_d$  sites reported so far suggest that the  $\text{Ni}_d$  site of the A-cluster is unlikely to participate in any redox process during catalysis and in turn imply that the  $\text{Ni}_p$  site is a candidate for reduction and CO binding during the ACS catalyzed reaction.<sup>19–25</sup> The  $\text{Ni}_c$  centers of the trinuclear species **6** and **8** are ligated to four metallosulfur ligands and hence resemble the  $\text{Ni}_p$  site to a

great extent. Both these models can be chemically reduced with reductants such as  $\text{Na}_2\text{S}_2\text{O}_4$  and  $\text{NaBH}_4$  at low temperature ( $-40^\circ\text{C}$ ) to afford EPR-active species. The X-band EPR spectrum of the reduced species  $\mathbf{6}_{\text{red}}$  in DMF glass (100 K) consists of an axial EPR signal ( $g = 2.33, 2.09$ ), while that of  $\mathbf{8}_{\text{red}}$  is more rhombic ( $g = 2.25, 2.12, 2.07$ ). Since **1** and **2** cannot be reduced by  $\text{Na}_2\text{S}_2\text{O}_4$  or  $\text{NaBH}_4$  (no EPR signal), it is evident that the  $\text{Ni(II)}_{\text{C}}$  centers in the trinuclear complexes undergo reduction. The similarity of the EPR spectra of  $\mathbf{6}_{\text{red}}$  and  $\mathbf{8}_{\text{red}}$  with those of other  $[\text{Ni(I)}\text{L}_4]$  species leads us to propose that the coordination geometry about the  $\text{Ni(I)}_{\text{C}}$  center in these reduced complexes is distorted tetrahedral.<sup>39</sup>

Passage of CO into DMF solutions of  $\mathbf{6}_{\text{red}}$  and  $\mathbf{8}_{\text{red}}$  results in the formation of their CO adducts that exhibit intense  $\nu_{\text{CO}}$  bands in their solution IR spectra at 1960 and 1971  $\text{cm}^{-1}$ , respectively. These  $\nu_{\text{CO}}$  values are consistent with terminal coordination of CO to the  $\text{Ni(I)}_{\text{C}}$  centers of  $\mathbf{6}_{\text{red}}\text{-CO}$  and  $\mathbf{8}_{\text{red}}\text{-CO}$  much like that proposed in ACS. The reduced  $\text{Ni(I)}\text{S}_4$  complex  $[\text{Ni}(\text{tpstd})]^-$  (tpstd = 2,2,11,11-tetraphenyl-1,5,8,12-tetrathiadodecane) with two alkanethiolato-S donors also binds CO in a similar manner and exhibits its  $\nu_{\text{CO}}$  value at 1940  $\text{cm}^{-1}$ .<sup>40</sup> The  $\nu_{\text{CO}}$  values for  $\mathbf{6}_{\text{red}}\text{-CO}$  and  $\mathbf{8}_{\text{red}}\text{-CO}$  are lower than that recorded for the enzyme (1996  $\text{cm}^{-1}$ ). This red-shift presumably arises from the enhanced electron density at the  $\text{Ni(I)}$  centers ligated by *four* metallosulfur donors (instead of the *three* observed in the enzyme) which in turn promotes more  $\pi$  back-donation to the  $\pi^*$  orbital of CO. The reduced species and their CO adducts are moderately stable at low temperatures. All efforts to isolate solids from the reaction mixtures have so far met with little success.

The Ni–Ni model complexes **9** and **10** provided the opportunity to study the reactions of CO with  $\text{Ni(I)}$  centers at modeled  $\text{M}_{\text{p}}$  sites (with different coordination geometries) as more accurate mimics of the bimetallic A-cluster subsite.<sup>27a</sup> When complex **9** with  $\text{N}_3\text{S}_2$  donor set at the  $\text{Ni}_{\text{p}}$  site is reduced with  $\text{Na}_2\text{S}_2\text{O}_4$  in DMF, the product exhibits an axial EPR spectrum with  $g = 2.23$  and 2.12 (Figure 12, top panel). This spectrum is nearly identical to the EPR spectra of  $[\text{Ni}^{\text{I}}(\text{terpy})(\text{SR})_2]^-$  species with distorted trigonal bipyramidal geometry.<sup>41</sup> It is therefore clear that  $\mathbf{9}_{\text{red}}$  retains its dinuclear structure and that the  $\text{Ni}_{\text{p}}$  center in **9** is reduced to the  $\text{Ni(I)}$  state. Passage of CO through the solution of  $\mathbf{9}_{\text{red}}$  in DMF affords  $\mathbf{9}_{\text{red}}\text{-CO}$  that exhibits a strong  $\nu_{\text{CO}}$  band in its solution IR spectrum at 2044  $\text{cm}^{-1}$ .

Since both **1** and **9** do not show any affinity toward CO, one can easily conclude that the  $\text{Ni(I)}$  center binds CO in  $\mathbf{9}_{\text{red}}\text{-CO}$ . The EPR spectrum of  $\mathbf{9}_{\text{red}}\text{-CO}$  is rhombic compared

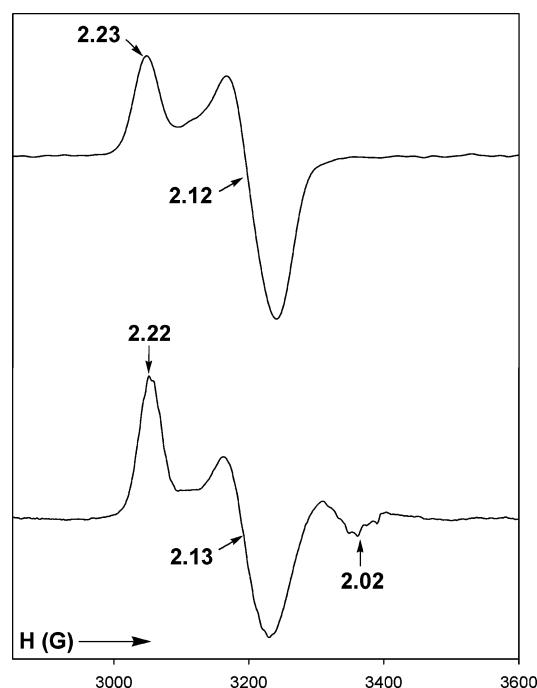


**Figure 12.** X-band EPR spectra of  $[\text{Ni}^{\text{I}}(\text{terpy})\text{Ni}^{\text{II}}(\text{NpPepS})]^-$  ( $\mathbf{9}_{\text{red}}$ , top) and  $[\text{Ni}^{\text{I}}(\text{terpy})(\text{CO})\text{Ni}^{\text{II}}(\text{NpPepS})]^-$  ( $\mathbf{9}_{\text{red}}\text{-CO}$ , bottom) in DMF glass at 100 K. Selected  $g$  values are indicated. Spectrometer settings: microwave frequency, 9.50 GHz; microwave power, 20 mW; modulation frequency, 100 kHz; modulation amplitude, 5 G.

to  $\mathbf{9}_{\text{red}}$  with  $g = 2.22, 2.13$ , and 2.02 (Figure 12, bottom panel) and resembles the EPR spectra of  $[\text{Ni}^{\text{I}}(\text{terpy})\text{-(SR)}_2(\text{CO})]^-$  species reported by this group.<sup>41</sup> For example, the  $\text{Ni(I)}$  complex  $[\text{Ni}^{\text{I}}(\text{terpy})(\text{C}_6\text{F}_5\text{S})_2(\text{CO})]^-$  exhibits a rhombic EPR signal in DMF glass with  $g = 2.20, 2.15$ , and 2.02 and displays  $\nu_{\text{CO}}$  band at 2045  $\text{cm}^{-1}$ .<sup>41c</sup> These data clearly indicate that the  $\text{Ni(I)}$  center in  $\mathbf{9}_{\text{red}}\text{-CO}$  exists in a distorted octahedral geometry and the CO is bound in a terminal fashion. The reduced complex,  $\mathbf{9}_{\text{red}}$ , and its CO-adduct,  $\mathbf{9}_{\text{red}}\text{-CO}$ , are moderately stable at low temperatures and decompose rapidly at room temperature. Prolonged passage of CO through DMF solutions of  $\mathbf{9}_{\text{red}}$  also affords  $[\text{Ni}^{\text{I}}(\text{terpy})(\text{CO})_2]^+$ .

Since the  $\text{Ni}_{\text{p}}$  site of ACS exists in a planar geometry in the structurally characterized (as isolated) enzyme,<sup>6,7</sup> the modeled  $\text{Ni}_{\text{p}}$  site of **10** was a more attractive target to study. It was expected that phosphine coordination to  $\text{Ni}_{\text{p}}$  in **10** would make the  $\text{Ni(I)}$  oxidation state accessible and result in a more stable CO adduct. Both expectations have been met with **10**. Complex **10** can be readily reduced by reductants such as  $\text{NaBH}_4$  and cobaltocene. The X-band EPR spectrum of  $\mathbf{10}_{\text{red}}$  is consistent with a distorted tetrahedral  $\text{Ni(I)}$  center with  $\text{P}_2\text{S}_2$  coordination and the resulting  $g$  values are close to 2.00 with significant hyperfine splitting originating from the two nonequivalent  $^{31}\text{P}$  nuclei of the dppe ligand frame.<sup>22,42</sup> The reduced species is quite stable at room

- (39) (a) Craft, J. L.; Mandimutsira, B. S.; Fujita, K.; Riordan, C. G.; Brunold, T. C. *Inorg. Chem.* **2003**, *42*, 859–867. (b) Musie, G.; Farmer, P. J.; Tuntulani, T.; Reibenspies, J. H.; Darensbourg, M. Y. *Inorg. Chem.* **1996**, *35*, 2176–2183.  
(40) Yamamura, T.; Sakurai, S.; Arai, H.; Miyamae, H. *J. Chem. Soc., Chem. Commun.* **1993**, 1656–1658.  
(41) (a) Marganian, C. A.; Vazir, H.; Baidya, N.; Olmstead, M. M.; Mascharak, P. K. *J. Am. Chem. Soc.* **1995**, *117*, 1584–1594. (b) Baidya, N.; Olmstead, M. M.; Whitehead, J. P.; Bagyinka, C.; Maroney, M. J.; Mascharak, P. K. *Inorg. Chem.* **1992**, *31*, 3612–3619. (c) Baidya, N.; Olmstead, M. M.; Mascharak, P. K. *Inorg. Chem.* **1991**, *30*, 929–937.

- (42) (a) James, T. L.; Cai, L.; Muetterties, M. C.; Holm, R. H. *Inorg. Chem.* **1996**, *35*, 4148–4161. (b) Kim, J. S.; Reibenspies, J. H.; Darensbourg, M. Y. *J. Am. Chem. Soc.* **1996**, *118*, 4115–4123. (c) James, T. L.; Smith, D. M.; Holm, R. H. *Inorg. Chem.* **1994**, *33*, 4869–4877. (d) Bowmaker, G. A.; Boyd, P. D. W.; Campbell, G. K. *Inorg. Chem.* **1982**, *21*, 2403–2412.



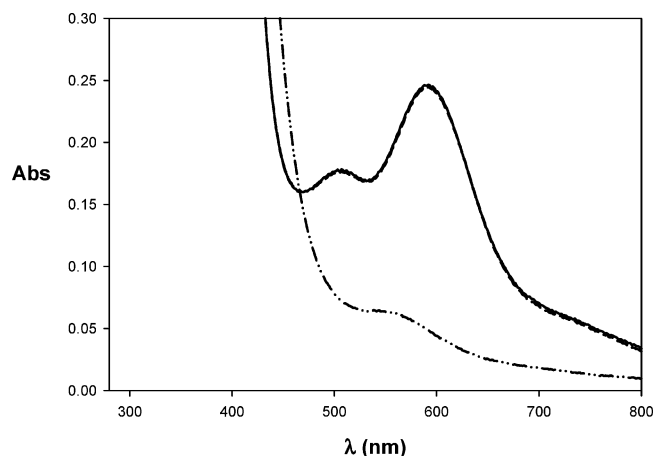


**Figure 13.** Electronic absorption spectrum of  $[\text{Ni}^{\text{II}}(\text{dppe})\text{Ni}^{\text{II}}(\text{PhPepS})]$  (**10**) (solid line) and its reduced species  $[\text{Ni}^{\text{I}}(\text{dppe})\text{Ni}^{\text{II}}(\text{PhPepS})]^-$  (**10<sub>red</sub>**) (dash-dotted line). Reoxidation of **10<sub>red</sub>** to **10** upon exposure to air in  $\text{CH}_2\text{Cl}_2$  is shown by the dashed line. The complex **10** was reduced with cobaltocene.

temperature. Under anaerobic conditions, one can monitor the reduction of **10** to **10<sub>red</sub>** in  $\text{CH}_2\text{Cl}_2$  with the use of 1 equiv of cobaltocene. Reaction of 1 equiv of cobaltocene with **10** affords **10<sub>red</sub>**, the species exhibiting the EPR spectrum. The violet color of **10** changes to light red-brown upon reduction. When the solution of **10<sub>red</sub>** in  $\text{CH}_2\text{Cl}_2$  is exposed to air, it is immediately reoxidized to **10** in nearly quantitative yield (Figure 13). This confirms that the  $(\mu\text{-SR})_2$  bridge remains intact during reduction.

Passage of CO through a solution of **10<sub>red</sub>** in  $\text{CH}_2\text{Cl}_2$  (or DMF) gives rise to the CO-adduct **10<sub>red</sub>-CO** that exhibits a strong  $\nu_{\text{CO}}$  band in its IR spectrum at  $1997\text{ cm}^{-1}$ , consistent with terminally bound CO to the  $\text{Ni}(\text{I})_{\text{p}}$  center. Complete removal of the solvent affords a dark red solid which also displays the same  $\nu_{\text{CO}}$  band in KBr matrix (Supporting Information).<sup>43</sup> Since the  $\nu_{\text{CO}}$  value of **10<sub>red</sub>-CO** is very close to the enzyme value of  $1996\text{ cm}^{-1}$ , it is reasonable to conclude that the  $\text{Ni}_{\text{p}}$  center in the enzyme binds CO in the +1 oxidation state. In  $\{[\text{Ni}(\text{CO})_2]\{[\text{NiS}_2\text{N}'_2]\}^{2-}$  (Figure 2a), two molecules of CO are bound to a  $\text{Ni}(\text{O})$  center in terminal fashion.<sup>24</sup> This  $\text{Ni}_{\text{p}}$  mimic displays two  $\nu_{\text{CO}}$  bands at  $1948$  and  $1866\text{ cm}^{-1}$ . Holm and co-workers have reported a  $\text{Ni}(\text{O})$  complex  $[\text{Ni}(\text{bpy})(\text{CO})_2]$  (bpy = 2,2'-bipyridine) which exhibits  $\nu_{\text{CO}}$  bands at  $1872$  and  $1973\text{ cm}^{-1}$  (KBr matrix).<sup>44</sup> Since these  $\nu_{\text{CO}}$  values are all lower than that displayed by **10<sub>red</sub>-CO**, it is evident that the latter species does contain  $\text{Ni}(\text{I})$  and not  $\text{Ni}(\text{O})$  at the  $\text{Ni}_{\text{p}}$  site. As mentioned above, the  $\text{Ni}_{\text{d}}$  site of **10** is quite resistant to reduction. Indeed, the  $\nu_{\text{CO}}$  values arising from the ligated carboxamido groups at the  $\text{Ni}_{\text{d}}$  sites of **10** and **10<sub>red</sub>-CO** are very close to each other and further support the presence of  $\text{Ni}(\text{II})$  at the  $\text{Ni}_{\text{d}}$  site in **10<sub>red</sub>-CO**.

The EPR spectrum of **10<sub>red</sub>-CO** in DMF glass is rhombic with  $g_1 = 2.20$ ,  $g_2 = 2.12$ ,  $g_3 = 2.05$ ; each line is split into

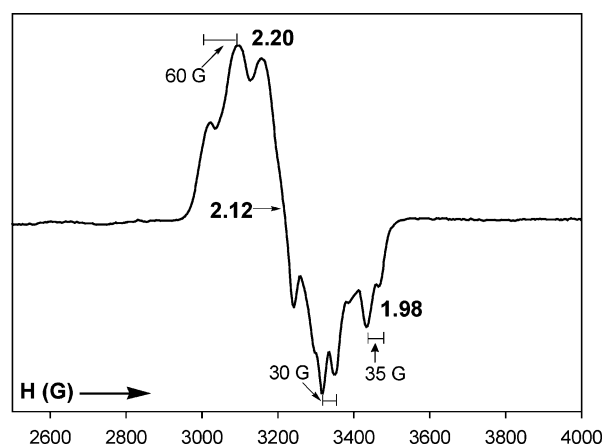


**Figure 14.** X-band EPR spectrum of  $[\text{Ni}^{\text{I}}(\text{dppe})(\text{CO})\text{Ni}^{\text{II}}(\text{PhPepS})]^-$  (**10<sub>red</sub>-CO**) in DMF glass at 100 K. Selected  $g$  and  $a$  values are indicated. Spectrometer settings: microwave frequency,  $9.50\text{ GHz}$ ; microwave power,  $20\text{ mW}$ ; modulation frequency,  $100\text{ kHz}$ ; modulation amplitude,  $5\text{ G}$ .

a triplet from coupling to two nonequivalent  $^{31}\text{P}$  nuclei (Figure 14). This spectrum resembles the EPR spectrum of  $[\text{Ni}(\text{psnet})]^+$ , a structurally characterized five-coordinate complex with distorted square pyramidal  $\text{P}_2\text{S}_2\text{N}$  ligation to a  $\text{Ni}(\text{I})$  center.<sup>42a</sup> The magnetic hyperfine interaction of  $^{31}\text{P}$  nuclei with an unpaired electron of  $\text{Ni}(\text{I})$  has been shown to be very susceptible to the coordination geometry around the metal center.<sup>42b</sup> For example, the EPR spectrum of the tetrahedral  $\text{Ni}(\text{I})$  complex  $[\text{Ni}(\text{PMe}_3)_4]^+$  (av  $\text{P-N-P}$  angle =  $109^\circ$ ) consists of an isotropic broad resonance with  $g = 2.12$  with no  $^{31}\text{P}$  hyperfine coupling<sup>45</sup> while the  $\text{Ni}(\text{I})$  complex  $[\text{Ni}(\text{psnet})]^+$  with distorted square pyramidal structure exhibits a rhombic EPR signal with  $g_1 = 2.21$ ,  $g_2 = 2.13$ , and  $g_3 = 2.01$  and  $a_1 = 45\text{ G}$ ,  $a_2 = 40\text{ G}$ , and  $a_3 = 44\text{ G}$ , respectively.<sup>42a</sup> In the present case, three distinct  $^{31}\text{P}$  hyperfine couplings with  $a$  values in the range of  $30\text{--}60\text{ G}$  are noted with **10<sub>red</sub>-CO** (Figure 14). We therefore assign a  $\{\text{NiP}_2\text{S}_2\text{-(CO)}\}-(\mu\text{-SR})_2-\{\text{Ni}^{\text{II}}(\text{N}_2\text{S}_2)\}$  formulation to **10<sub>red</sub>-CO**.

Recently, three groups have reported sulfur-bridged dinuclear  $\text{Ni}$  complexes with  $\text{P}_2\text{S}_2$  coordination<sup>19,20a,22</sup> at the bridged  $\text{Ni}$  center ( $\text{Ni}_{\text{p}}$  mimic) that exhibit low  $\text{Ni}(\text{I})/\text{Ni}(\text{II})$  redox potentials.<sup>20,22</sup> Unfortunately, very little spectroscopic data are currently available on the CO adducts of these complexes in the reduced state. Complex **10** deserves attention in this regard as the first structurally characterized  $\text{Ni-Ni}$  model that includes dicarboxamido-dithiolato ligation ( $\text{Ni}_{\text{d}}$  mimic) to a bridged  $\text{Ni}(\text{II})$  center that (i) can be reduced to the  $\text{Ni}(\text{I})$  state and (ii) binds CO in the reduced state ( $\text{Ni}_{\text{p}}$  mimic) much like that proposed for the A-cluster of ACS/CODH.

In the absence of the  $\text{Fe}_4\text{S}_4$  portion of the A-cluster in the sulfur-bridged  $\text{Ni-Ni}$  models, it is impossible to assess the effect(s) of the iron-sulfur cluster on the chemical and redox properties of the  $\text{Ni}_{\text{p}}$  center. Although recent studies have indicated that electron flow to and from the  $\text{Fe}_4\text{S}_4$  cluster is too slow compared to the rate of methyl transfer,<sup>46</sup> the

(43) The red solid is moderately stable under anaerobic conditions; however, it decomposes slowly in solution and, to date, we have not been able to characterize it by structural studies. The EPR spectrum of a solution of the freshly isolated red solid in DMF (same as Figure 14) confirms that the solid is indeed **10<sub>red</sub>-CO**.

(44) Tucci, G. C.; Holm, R. H. *J. Am. Chem. Soc.* **1995**, *117*, 6489–6496.

(45) Gleizes, A.; Dartiguenave, M.; Dartiguenave, Y.; Galy, J.; Klein, H. F. *J. Am. Chem. Soc.* **1977**, *99*, 5187–5189.

(46) Tan, X.; Sewell, C.; Yang, Q.; Lindahl, P. A. *J. Am. Chem. Soc.* **2003**, *125*, 318–319.

proposed mechanisms of ACS activity mostly involve redox changes at the  $\text{Fe}_4\text{S}_4$  cluster during key steps of the catalytic cycle.<sup>5,6,47,48</sup> Theoretical studies suggest that the  $\text{Ni}(0)$  state<sup>49</sup> is only stabilized by either removal of the cluster<sup>15</sup> or by the presence of a neighboring reduced iron–sulfur cluster  $[\text{Fe}_4\text{S}_4]^{1+}$  ( $S = 1/2$ ).<sup>48</sup> Clearly, the next generation models of the ACS A-cluster have to incorporate the  $\text{Fe}_4\text{S}_4$  cluster in order to address these issues.<sup>47,50</sup> Such attempts are in progress in this laboratory at this time.

## Conclusions

The results of the modeling work reported here reveal valuable insight into the novel A-cluster site involved in acetyl CoA synthesis by ACS/CODH. For example, it is quite evident that coordination of both carboxamido nitrogen and thiolato sulfur stabilizes the  $\text{Ni}(\text{II})$  state to a great extent (like in **1** and **2**) and hence the  $\text{Ni}_d$  site in the enzyme is not expected to participate in any redox chemistry. Binding of potential substrates such as CO at this site is also unlikely. Furthermore,  $\text{Ni}(\text{II})$  centers bridged to metallosulfur moieties

( $\text{Ni}_p$  mimics) appear quite capable of binding substrates such as CO when in the reduced  $\text{Ni}(\text{I})$  state but not in the  $\text{Ni}(\text{II})$  state. The IR spectra of such CO adducts exhibit  $\nu_{\text{CO}}$  bands in the range 1960–2044  $\text{cm}^{-1}$ , indicating terminal  $\text{Ni}(\text{I})$ –CO coordination similar to that proposed in the enzyme ( $\nu_{\text{CO}} = 1996 \text{ cm}^{-1}$ ). Since the  $\text{Ni}$ – $\text{Ni}$  models of this work (such as **9** and **10**) are devoid of the strong dipolar coupling of the  $\text{Ni}_p$  site to the  $\text{Fe}_4\text{S}_4$  cluster, the EPR spectra of the CO-adducts such as **10**<sub>red</sub>–CO do not resemble the  $\text{NiFeC}$  EPR signal. The removal of  $\text{Ni}_p$  sites from selected models by phen provides strong evidence in favor of  $\text{Ni}_p$  being the source of “labile Ni” in the enzyme. No reactivity toward CO has been noted with the dinuclear  $\text{Ni}$ – $\text{Cu}$  models (**3** and **4**). Collectively, these observations lend support to the present notion that the  $\text{M}_p$  site in catalytically active ACS/CODH is occupied by Ni.

**Acknowledgment.** T.C.H. received financial support from NIH IMSD Grant No. GM58903.

**Supporting Information Available:** FTIR spectra of **10** and **10**<sub>red</sub>–CO in KBr matrix (Figure S1), machine parameters, crystal data, and data collection parameters for all the complexes (Table S1), selected bond distances and angles are reported (Table S2), and X-ray crystallographic data (in CIF format) and tables for the structure determination of complexes **2**, **3**·0.5 $\text{Et}_2\text{O}$ ·0.5 $\text{H}_2\text{O}$ , **4**· $\text{H}_2\text{O}$ , **5**·DMF, **6**·3DMF, **8**, and **10**· $\text{CH}_2\text{Cl}_2$ . This material is available free of charge via the Internet at <http://pubs.acs.org>.

IC0520465

(47) Hegg, E. L. *Acc. Chem. Res.* **2004**, *37*, 775–783.

(48) Amara, P.; Volbeda, A.; Fontecilla-Camps, J. C.; Field, M. J. *J. Am. Chem. Soc.* **2005**, *127*, 2776–2784.

(49) Lindahl, P. A. *J. Biol. Inorg. Chem.* **2004**, *9*, 516–524.

(50) In a recent paper, Holm and co-workers have reported the results of such an attempt. However, only complexes of the thiolato-bridged  $[\text{Fe}_4\text{S}_4]\text{-NiL}$  type have been isolated. See: Rao, P. V.; Bhaduri, S.; Jiang, J.; Hong, D.; Holm, R. H. *J. Am. Chem. Soc.* **2005**, *127*, 1933–1945.